Nuclear Physics A531 (1991) 253–284
North-Holland

FRAGMENTATION OF SINGLE-PARTICLE STRENGTH AND THE VALIDITY OF THE SHELL MODEL*

M.G.E. BRAND, G.A. RIJSDIJK, F.A. MULLER and K. ALLAART

Department of Physics and Astronomy, Free University, De Boelelaan 1081, 1081 HV Amsterdam, The Netherlands

W.H. DICKHOFF

Department of Physics, Washington University, St. Louis, MO 63130, USA

Received 27 July 1990
(Revised 22 March 1991)

Abstract: The problem of missing spectroscopic strength in proton knock-out reactions is addressed by calculating this strength with a realistic interaction up to about a hundred MeV missing energy. An interaction suitably modified for short-range correlations (*G*-matrix) is employed in the calculation of the self-energy including all orbitals up to and including three major shells above the Fermi level for protons. The spectroscopic strength is obtained by solving the Dyson equation for the Green function with a self-energy up to second order in the interaction. Results for ^{48}Ca and ^{90}Zr are compared with recent (e, e'p) data. The calculated strength overestimates the data by about 10–15% of the independent particle shell-model (IPSM) sum rule. This is in accordance with what is expected from depletions calculated in infinite nuclear matter. Inclusion of higher order terms into the self-energy, especially the correlated motion of particles and holes, is found to be necessary to reproduce the observed fragmentation of strength in the low-energy region. The widths of the strength distributions compare well with empirical formulas which have been deduced from optical potentials. The validity of the conventional shell-model picture is connected with the relevance of Landau's quasiparticle picture for strongly interacting Fermi systems.

1. Introduction

The interest in nuclear spectral functions has been revived by recent accurate (e, e'p) data [1–4]. The knock-out from specific shell-model orbits has now been very well identified, also for heavy nuclei. From the analysis of these data it came out somewhat as a surprise that the total observed spectroscopic strength for orbits below the Fermi level amounts to only 50–70% of the independent particle shell-model (IPSM) sum rule. This has raised the question whether the depletion of orbits

* This work is part of the research program of the Foundation for Fundamental Research of Matter (FOM), which is financially supported by the Netherlands' Organization for Scientific Research (NWO). It was also partially supported by the Condensed Matter Theory Program of the Division of Materials Research of the U.S. National Science Foundation under Grant No. DMR-9002863 (at Washington University). Computer time was supplied by the Foundation SURF from the Netherlands' National Fund use Supercomputers(NSF).

below the Fermi level, in magic nuclei, may indeed be as large as 30–50% or whether there is a large fraction of the strength still undetected at higher missing energies.

Several authors have addressed this question recently [5-7]). Part of the answer may be found in the effect of short-range correlations. Most calculations using realistic short-range forces have been performed for infinite nuclear matter (NM). These results are also relevant for finite nuclei, since the short-range repulsive forces scatter particles into states far above the Fermi level and this process is hardly affected by the presence of the rather dilute nuclear medium. The depletion of states by these short-range correlations is expected to be somewhat less for finite nuclei than for nuclear matter at normal density ($k_F = 1.4\,\mathrm{fm}^{-1}$) since the average density for finite nuclei is lower. The effect of short-range correlations in nuclear matter can be well calculated with realistic interactions. This one may conclude from the fact that similar results have been obtained with different methods. Ramos *et al.* [6]) have calculated the self-energy including the effect of short-range correlations. The spectral functions are obtained by solving the Dyson equation and are found to span an energy domain of several GeV. With a semi-realistic interaction derived from Reid's soft-core potential these authors find about 13% depletion of states below the Fermi level for normal nuclear matter density due to the influence of short-range correlations. This removed single-particle (s.p.) strength is found as particle strength in a smooth distribution out to very high energy as a result of the short-range correlations. The hole strength is found to be mainly concentrated around the quasiparticle peak and only a few percent is obtained at higher missing energy. Similar results were obtained using the method of correlated basis functions [7]). In these calculations also the effect of tensor forces was included, as a consequence of which a somewhat larger depletion of about 20% is found. In addition a somewhat larger background contribution to the hole strength is observed, which does not exceed 10%, however. These depletions can in principle be related to the parameter κ in the hole-line expansion [8]) which yields similar results for the wound integral [9]). In finite nuclei, such as ^{16}O, ^{40}Ca and ^{48}Ca, which have a smaller average density than nuclear matter, one may therefore expect a depletion of shell-model orbits by short-range and tensor correlations of roughly 10–15%.

In addition to these correlations due to the short-range and tensor interactions, there are correlations caused by the long-range components of the NN force. Also induced forces, such as those arising from phonon exchange may enhance correlation phenomena. For these phonons, by which we understand excitations of the nucleus up to about 100 MeV, the finite size of the nucleus plays an essential role. This finite size is the origin of shell effects and gives rise to a variety of surface excitations. The influence of these long-range forces on spectral functions must therefore be calculated explicitly in finite nuclei. It is the aim of the present paper to contribute to the investigation of this aspect. Only the influence of excitations up to about 100 MeV on the spectral functions will be considered in this work. The influence of short-range and tensor correlations should therefore still be added to the results

presented here. As a reasonable starting point for the effective NN interaction a Brueckner G-matrix is used which has proven to be very useful in finite nucleus calculations.

The importance of the dynamic coupling between particle motion and nuclear excitations at low energy, up to a hundred MeV, and the corresponding signature of the breakdown of the mean field picture is observed when protons or neutrons are knocked out of shells far from the Fermi level. Recent (p, 2p) and (p, pn) experiments on ^{16}O show this for the lowest $s_{1/2}$ shell which exhibits a broad energy distribution in contrast to the $p_{3/2}$ and $p_{1/2}$ states close to the Fermi energy [10]. This is similar to the older Saclay results obtained with electrons [11]. A similar picture emerges from the (e, e'p) results on ^{40,48}Ca [ref. [3]], ^{90}Zr [ref. [1]] and ^{208}Pb [ref. [2]]. This broadening of states which in a Hartree–Fock picture are far removed from the Fermi energy, indicates clearly that hole states at those energies can mix readily with more complicated states like two-hole–one-particle states which are abundantly present. This same mixing occurs for states near the Fermi energy, although it does not result in broadening since the density of more complicated states is very low there, due to the gap in the single-particle spectrum. Instead, the mixing leads to a reduction of the hole strength, as is experimentally observed. Therefore the single-particle energy gap plays an important role in increasing the validity of the shell-model concept, as we shall illustrate.

As a tool for our investigations we shall employ the Green function method, which is also well suited to describe the nuclear response beyond a mean-field approximation as discussed recently [12]. In sect. 2 we discuss an approximation to the self-energy which treats the coupling to 2p1h and 1p2h states. With the interaction and model space given in sect. 3 the spectral functions of ^{48}Ca and ^{90}Zr are calculated. These results are presented in sects. 4 and 5, respectively. Both nuclei have recently been investigated by means of the (e, e'p) reaction [1,3]. Older calculations of this type [13–15] have concentrated mainly on ^{16}O and the cross section for knock-out reactions. In addition, simple zero-range interactions were used in refs. [14,15]. The calculated fragmentation of the spectroscopic strength at low energy is compared with the experimental observations and a prediction is given for the amount of strength at higher missing energies, as well as for the depletion by the effects of long-range forces. This is done for ^{48}Ca in sect. 4 and ^{90}Zr in sect. 5. In sect. 6 contact is made with empirical results describing the width of the hole states and the imaginary part of the optical potential for states above the Fermi energy. Sect. 7 contains more general comments and conclusions concerning the fragmentation of spectral strength and its implications for the validity of the shell model.

2. Spectral functions and single-particle propagator

Experimentally the motion of nucleons in shell-model orbits may be investigated with knock-out reactions such as (e, e'p), (p, 2p) and (p, pn). From these one deduces

the probability for removing a nucleon from its orbit α in the ground state of the nucleus with A particles ending up in the nth state of the $A-1$ system with energy E_n^{A-1} ($n=0$ denotes the ground state). This probability determines the hole spectral function

$$S_h(\alpha,\omega)=\sum_{n=0}|\langle\Psi_n^{A-1}|a_\alpha|\Psi_0^A\rangle|^2\delta(\omega-(E_0^A-E_n^{A-1}))\,. \tag{2.1}$$

In the IPSM description of the nuclear ground state the hole spectral function (2.1) would have only contributions with weight equal to unity at energies $\omega=\varepsilon_\alpha$ corresponding to the s.p. energies of the occupied states in the non-interacting approximation to the ground state. In reality (2.1) consists of many fragments for the various excited states, including the continuum of the $A-1$ nucleus. It is therefore clear that the IPSM should be corrected for correlations.

The occupation probability of the orbit α in the ground state of the A-nucleus is given by the integrated hole spectral function:

$$n(\alpha)=\int_{-\infty}^{\varepsilon_F^-}d\omega\,S_h(\alpha,\omega)\,. \tag{2.2}$$

Here the upper limit is the particle removal energy

$$\varepsilon_F^-=E_0^A-E_0^{A-1}\,. \tag{2.3}$$

The integration in (2.2) may be extended up to infinity, however, as S_h is zero for $\omega>\varepsilon_F^-$.

One defines similarly the particle spectral function corresponding to processes where a particle is added to the A-nucleon system:

$$S_p(\alpha,\omega)=\sum_{n=0}|\langle\Psi_n^{A+1}|a_\alpha^\dagger|\Psi_0^A\rangle|^2\delta(\omega-(E_n^{A+1}-E_0^A))\,. \tag{2.4}$$

The emptiness of orbit α is obtained by integration of this particle spectral function

$$1-n(\alpha)=\int_{\varepsilon_F^+}^{\infty}d\omega\,S_p(\alpha,\omega)\,. \tag{2.5}$$

Here the lower limit of integration is given by

$$\varepsilon_F^+=E_0^{A+1}-E_0^A\,. \tag{2.6}$$

In infinite systems without pairing correlations the energies (2.3) and (2.6) coincide and are equal to the Fermi energy ε_F.

These spectral functions may be calculated from the single-particle propagator in the exact ground state. Consider the hamiltonian

$$H=\sum_{\alpha\beta}\langle\alpha|T|\beta\rangle a_\alpha^\dagger a_\beta+\tfrac{1}{4}\sum_{\alpha\beta\gamma\delta}\langle\alpha\beta|V|\gamma\delta\rangle a_\alpha^\dagger a_\beta^\dagger a_\delta a_\gamma \tag{2.7}$$

in which T is the kinetic energy operator, V an effective nucleon–nucleon interaction, and the operators $a_\alpha^\dagger(a_\alpha)$ denote particle creation (annihilation) operators in the

s.p. states $|\alpha\rangle$ ($\alpha = n_a, l_a, j_a, m_a$), which form a complete set of single-particle orbits. As discussed in the Introduction, the interaction will be of G-matrix type, suitably approximated as a static interaction. As the results presented in this formalism have general validity we shall use the symbol V.

Often one makes a separation:

$$H = (T+U)+(V-U) = H_0+(V-U) \tag{2.8}$$

in which U is chosen a suitable mean field potential (e.g. Hartree-Fock, harmonic oscillator or Woods-Saxon). Since it is a one-body potential for which the above-mentioned single-particle orbits are supposed to be the eigenstates, this leads only to a trivial extension of the formulas presented in this section.

The exact ground state $|\Psi_0\rangle$ of eq. (2.7) may be formally written as a perturbation expansion in the interaction V [refs. [16,17])]. It is assumed here that this ground state refers to a doubly magic nucleus. The single-particle propagator is defined as

$$ig_{\alpha\beta}(t-t') = \frac{\langle \Psi_0^A | \mathrm{T}[a_\alpha(t) a_\beta^\dagger(t')] | \Psi_0^A \rangle}{\langle \Psi_0^A | \Psi_0^A \rangle}, \tag{2.9}$$

in which T represents the time-ordering operation, $|\Psi_0^A\rangle$ is the Heisenberg A-particle ground state of the interacting system satisfying

$$H|\Psi_0^A\rangle = E_0|\Psi_0^A\rangle \tag{2.10}$$

and $a_\alpha(t)$ is a Heisenberg operator with the time dependence

$$a_\alpha(t) = \mathrm{e}^{iHt} a_\alpha \, \mathrm{e}^{-iHt}. \tag{2.11}$$

Note that $\hbar$ is set equal to 1.

The single-particle propagator characterizes the propagation of a state containing an additional particle (for $t > t'$) or a state with a removed particle (for $t < t'$). It contains information about the expectation value of any single-particle operator in the ground state of the system [16]), e.g. the charge density, and the ground-state energy when the interaction is of two-body nature. Besides this it contains information about the excited states of the system which are obtained by adding or removing a particle. This latter property is demonstrated clearly by inserting a complete set of $A+1$ ($|\Psi_n^{A+1}\rangle$) and $A-1$ ($|\Psi_n^{A-1}\rangle$) eigenstates of the hamiltonian H, introducing the integral representation of the step function and performing the time Fourier transform over $t-t'$. In this way one obtains the spectral or Lehmann representation of the s.p. propagator:

$$g_{\alpha\beta}(\omega) = \sum_n \frac{\langle \Psi_0^A | a_\alpha | \Psi_n^{A+1} \rangle \langle \Psi_n^{A+1} | a_\beta^\dagger | \Psi_0^A \rangle}{\omega - (E_n^{A+1} - E_0^A) + i\eta} + \sum_m \frac{\langle \Psi_0^A | a_\beta^\dagger | \Psi_m^{A-1} \rangle \langle \Psi_m^{A-1} | a_\alpha | \Psi_0^A \rangle}{\omega - (E_0^A - E_m^{A-1}) - i\eta}. \tag{2.12}$$

From this representation one can infer that the poles of (2.12) correspond to the exact excitation energies of the $A+1$ and $A-1$ states with respect to the ground state of the system of A particles, while the residues at these poles contain the

corresponding transition amplitudes. It is important to note that (2.12) contains this information for all states with non-zero transition amplitudes, e.g. also for those which have predominantly 2p1h (1p2h) or more complex nature.

The relation between the spectral functions and the single-particle propagator is evident from (2.12). One obtains:

$$S_h(\alpha, \omega) = \lim_{\eta \to 0} \frac{1}{\pi} \operatorname{Im} g_{\alpha\alpha}(\omega) ; \qquad \omega < \varepsilon_F^- \tag{2.13}$$

and

$$S_p(\alpha, \omega) = \lim_{\eta \to 0} \frac{-1}{\pi} \operatorname{Im} g_{\alpha\alpha}(\omega) ; \qquad \omega > \varepsilon_F^+ . \tag{2.14}$$

The s.p. propagator satisfies the well-known Dyson equation [16,17]), which in the energy representation is written as

$$g_{\alpha\beta}(\omega) = g^{(0)}_{\alpha\beta}(\omega) + \sum_{\gamma\delta} g^{(0)}_{\alpha\gamma}(\omega) \Sigma^*_{\gamma\delta}(\omega) g_{\delta\beta}(\omega) \tag{2.15}$$

and graphically represented in fig. 1. Considering the equation of motion of the s.p. propagator it is possible to obtain an algebraic expression for the irreducible self-energy, Σ^*, in terms of the vertex function, Γ, which consists of all possible interaction diagrams between two dressed particles [17]). Any approximation to Γ then automatically leads to a self-consistent formulation of the calculation of the s.p. propagator. This method is referred to as self-consistent Green function (SCGF) theory. Neglecting Γ results in no dynamic coupling between the particles and only the lowest order in V contributes to the self-energy in this approximation. This is the self-consistent Hartree–Fock (HF) self-energy $\Sigma^{(1)}$, depicted in fig. 2a, and written as

$$\Sigma^{(1)}_{\alpha\beta} = \sum_{\mu\nu} \langle \alpha\mu | V | \beta\nu \rangle \langle \Psi_0(\mathrm{HF}) | a^\dagger_\nu a_\mu | \Psi_0(\mathrm{HF}) \rangle . \tag{2.16}$$

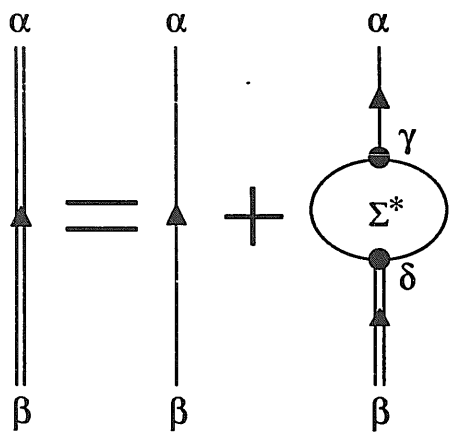

Fig. 1. Graphical representation of the Dyson eq. (2.15). The double arrows represent the fully dressed single-particle propagator g.

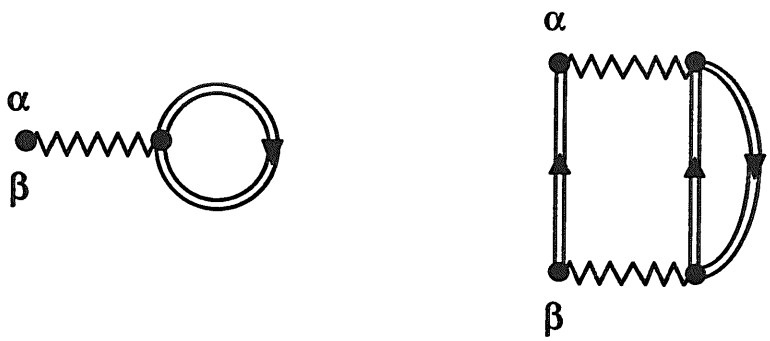

Fig. 2. Two diagrams which are considered here. Diagram (a) represents the self-consistent HF diagram (exchange included) and diagram (b) the second-order self-consistent self-energy diagram.

The HF field is static and leads to a ground state described by a single Slater determinant. In the HF s.p. basis the s.p. propagator is diagonal:

$$g^{(1)}_{\alpha\beta}(\omega)=\delta_{\alpha\beta}\left[\frac{\theta(\alpha-F)}{\omega-\varepsilon^{\mathrm{HF}}_{\alpha}+i\eta}+\frac{\theta(F-\alpha)}{\omega-\varepsilon^{\mathrm{HF}}_{\alpha}-i\eta}\right]. \tag{2.17}$$

From now on we will assume to be working in the HF basis.

The next higher-order self-consistent problem is defined by approximating the vertex function by V. This results in the second-order self-consistent self-energy (fig. 2b):

$$\Sigma^{(2)}_{\alpha\beta}(\omega)=\tfrac{1}{2}\sum_{\mu\nu\kappa\lambda\gamma\delta}\int\frac{\mathrm{d}\omega_1}{2\pi i}\int\frac{\mathrm{d}\omega_2}{2\pi i}$$
$$\times\langle\alpha\delta|V|\mu\kappa\rangle\langle\nu\lambda|V|\beta\gamma\rangle g^{(2)}_{\mu\nu}(\omega-\omega_1+\omega_2)g^{(2)}_{\kappa\lambda}(\omega_1)g^{(2)}_{\gamma\delta}(\omega_2)\}\,, \tag{2.18}$$

in which the s.p. propagator $g^{(2)}$ satisfies

$$g^{(2)}_{\alpha\beta}(\omega)=g^{(1)}_{\alpha\beta}(\omega)+\sum_{\gamma\delta}g^{(1)}_{\alpha\gamma}(\omega)\Sigma^{(2)}_{\gamma\delta}(\omega)g^{(2)}_{\delta\beta}(\omega)\,. \tag{2.19}$$

Due to the explicit energy dependence of $\Sigma^{(2)}$, this poses a very difficult self-consistency problem. This is illustrated clearly by considering for the moment only the lowest order contribution to $\Sigma^{(2)}$ which is obtained by replacing $g^{(2)}$ by $g^{(1)}$ in (2.18). One then can evaluate the integrals in (2.18) obtaining:

$$\Sigma^{(2)\mathrm{HF}}_{\alpha\beta}(\omega)=\tfrac{1}{2}\sum_{J}\frac{(2J+1)}{(2j_{\mathrm{a}}+1)}\sum_{\mu\nu\kappa}\langle\alpha\kappa J|V|\mu\nu J\rangle\langle\mu\nu J|V|\beta\kappa J\rangle$$
$$\times\left\{\frac{\theta(\mu-F)\theta(\nu-F)\theta(F-\kappa)}{\omega-(\varepsilon^{\mathrm{HF}}_{\mu}+\varepsilon^{\mathrm{HF}}_{\nu}-\varepsilon^{\mathrm{HF}}_{\kappa})+i\eta}+\frac{\theta(F-\mu)\theta(F-\nu)\theta(\kappa-F)}{\omega-(\varepsilon^{\mathrm{HF}}_{\mu}+\varepsilon^{\mathrm{HF}}_{\nu}-\varepsilon^{\mathrm{HF}}_{\kappa})-i\eta}\right\}. \tag{2.20}$$

This self-energy describes the coupling of particles and holes to unperturbed 2p1h and 1p2h states. The two contributions to (2.20) are represented in fig. 3, using the time-ordered Goldstone diagrams.

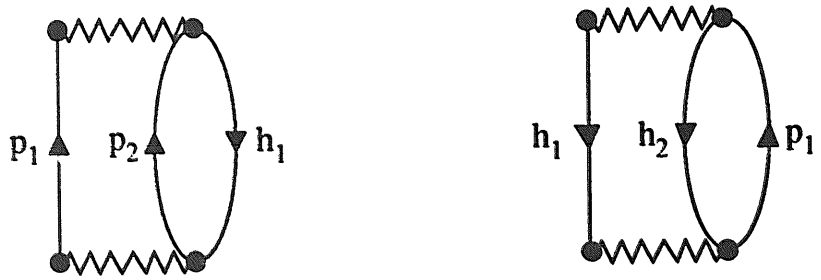

Fig. 3. The second-order self-energy $\Sigma^{(2)HF}$, eq. (2.20) represented by Goldstone diagrams. The single-particle lines represent the HF propagators with the convention that up-going lines represent particle states (p_1, p_2) and down-going lines represent hole states (h_1, h_2).

Working in a discrete basis one can solve the Dyson equation with self-energy (2.20) by explicitly calculating the poles and the corresponding residues of the s.p. propagator. Inserting the Lehmann representations (2.12) and (2.17) into (2.19), multiplying by $\omega-(E_n^{A+1}-E_0^A)$ and taking the limit $\omega\to E_n^{A+1}-E_0^A$ one obtains an eigenvalue equation for the excitation energies $E_n^{A+1}-E_0^A$ and corresponding spectral strengths:

$$\sum_\beta(\delta_{\alpha\beta}\varepsilon_\alpha^{HF}+\Sigma_{\alpha\beta}^{(2)HF}(E_n^{A+1}-E_0^A))\langle\Psi_n^{A+1}|a_\beta^\dagger|\Psi_0^A\rangle=(E_n^{A+1}-E_0^A)\langle\Psi_n^{A+1}|a_\alpha^\dagger|\Psi_0^A\rangle \tag{2.21}$$

in which the transition amplitudes have to be normalized by a condition that can also be obtained from the Dyson equation:

$$\sum_\alpha|\langle\Psi_n^{A+1}|a_\alpha^\dagger|\Psi_0^A\rangle|^2=1+\sum_{\alpha\beta}\langle\Psi_0^A|a_\alpha|\Psi_n^{A+1}\rangle\langle\Psi_n^{A+1}|a_\beta^\dagger|\Psi_0^A\rangle\left.\frac{d\Sigma_{\alpha\beta}^{(2)HF}(\omega)}{d\omega}\right|_{\omega=E_n^{A+1}-E_0^A}. \tag{2.22}$$

A similar set of equations is obtained for the excitation energies $E_0^A-E_n^{A-1}$ and corresponding transition amplitudes by multiplying by $\omega-(E_0^A-E_n^{A-1})$ and taking the limit $\omega\to E_0^A-E_n^{A-1}$:

$$\sum_\beta(\delta_{\alpha\beta}\varepsilon_\alpha^{HF}+\Sigma_{\alpha\beta}^{(2)HF}(E_0^A-E_n^{A-1}))\langle\Psi_n^{A-1}|a_\beta|\Psi_0^A\rangle=(E_0^A-E_n^{A-1})\langle\Psi_n^{A-1}|a_\alpha|\Psi_0^A\rangle \tag{2.23}$$

and

$$\sum_\alpha|\langle\Psi_n^{A-1}|a_\alpha|\Psi_0^A\rangle|^2=1+\sum_{\alpha\beta}\langle\Psi_0^A|a_\beta^\dagger|\Psi_n^{A-1}\rangle\langle\Psi_n^{A-1}|a_\alpha|\Psi_0^A\rangle\left.\frac{d\Sigma_{\alpha\beta}^{(2)HF}(\omega)}{d\omega}\right|_{\omega=E_0^A-E_n^{A-1}}. \tag{2.24}$$

The set of eqs. (2.21)-(2.24) can be solved by calculating the eigenvalue curves $E(\omega)$ of the eigenvalue equation

$$\sum_\beta(\delta_{\alpha\beta}\varepsilon_\alpha^{HF}+\Sigma_{\alpha\beta}^{(2)HF}(\omega))X_\beta(\omega)=E(\omega)X_\alpha(\omega) \tag{2.25}$$

and crossing these curves with the line $\omega = E(\omega)$. This is illustrated in fig. 4. The solutions $E(\omega) < \varepsilon_F^-$ correspond to the excitation energies $E_0^A - E_n^{A-1}$ and the solutions $E(\omega) > \varepsilon_F^+$ correspond to the excitation energies $E_n^{A+1} - E_0^A$. The corresponding eigenvectors can be normalized by the conditions given in eqs. (2.22) and (2.24), which show that the spectral strength is determined by the slope of the eigenvalue curve. The self-energy should conserve angular momentum (which implies $l_a, j_a = l_b, j_b$ in (2.18) and (2.20)), and then the dimensions of the self-energy matrices are very small (not larger than 4 by 4 in the model spaces considered) so that all solutions can be obtained easily with high accuracy.

Because the diagonal self-energy $\Sigma_{\alpha\alpha}^{(2)HF}$ is a monotonically decreasing function of ω between each two successive poles (as it should be to satisfy the normalization condition), the eigenvalue curve always crosses the line $\omega = E(\omega)$, so that between each two poles a solution is obtained. The majority of these solutions are found very close to the 2p1h or 1p2h poles and these 2p1h- and 1p2h-like solutions have therefore only a small spectroscopic strength. Due to the large number of 2p1h and 1p2h states (typically a few thousand in the model spaces considered), the single-particle strength becomes strongly fragmented.

The coupling of hole states to 2p1h states will lead to a depletion of the hole states, while the coupling of the particle states to the 1p2h states leads to a filling of the particle states. In order to conserve the particle number these two effects have to compensate each other, which is one of the reasons why one should solve the Dyson equation self-consistently [12]). This would mean that the solution obtained

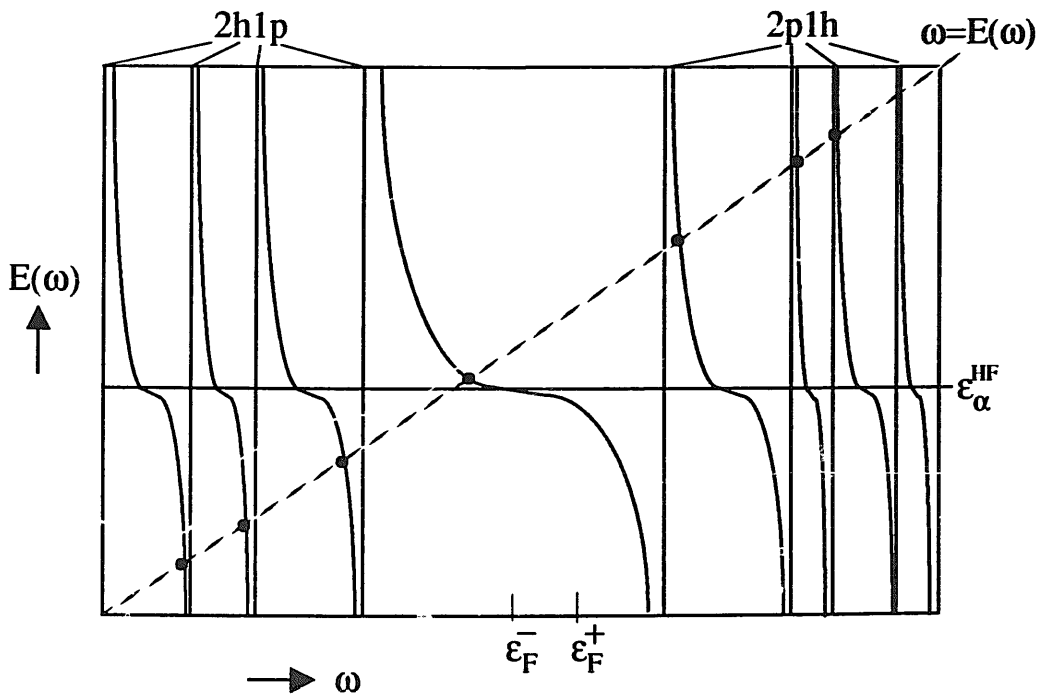

Fig. 4. Illustration of the procedure to find the self-consistent eigenvalues of eq. (2.25) for the case of a one-dimensional self-energy. The black dots denote the self-consistent solutions (see text).

with the self-energy (2.20), should be substituted back into the expression for the self-energy (2.20). This would increase the number of poles (and thus of solutions) to roughly the cube of the number one already obtains with (2.20). Iterating such a scheme to convergency is clearly not feasible due to the numerical complexity. To simplify the calculation it is suggested to replace $g^{(2)}$ in (2.18) by the single-pole approximation:

$$g^{(2)}_{\alpha\beta}(\omega) \approx \delta_{\alpha\beta}\left[\frac{\theta(\alpha - F)}{\omega - \varepsilon_\alpha + i\eta} + \frac{\theta(F-\alpha)}{\omega - \varepsilon_\alpha - i\eta}\right]. \tag{2.26}$$

The single-pole energies ε_α are then related to the empirical quasiparticle energies for states near the Fermi level, while for states far from the Fermi energy the single-pole energies can be considered as "mean removal energies [18]). With this approximation the second-order self-energy becomes:

$$\Sigma^{(2)}_{\alpha\beta}(\omega) = \tfrac{1}{2}\sum_J \frac{(2J+1)}{(2j_\alpha+1)} \sum_{\mu\nu\kappa} \langle \alpha\kappa J|V|\mu\nu J\rangle\langle \mu\nu J|V|\beta\kappa J\rangle$$
$$\times\left\{\frac{\theta(\mu-F)\theta(\nu-F)\theta(F-\kappa)}{\omega-(\varepsilon_\mu+\varepsilon_\nu-\varepsilon_\kappa)+i\eta} + \frac{\theta(F-\mu)\theta(F-\nu)\theta(\kappa-F)}{\omega-(\varepsilon_\mu+\varepsilon_\nu-\varepsilon_k)-i\eta}\right\}, \tag{2.27}$$

and the Dyson equation can be solved with the procedure sketched above.

The choice for the ε_α's is discussed in more detail in sect. 3. As mentioned at the end of sect. 4, the violation of the particle number, due to the lack of self-consistency, is then found to be very small.

3. Interaction and model space

3.1. INTERACTION

As we shall perform our calculations within a limited shell-model configuration space, this space is insufficient to accommodate correlations due to the short-range repulsion, which is present in realistic NN potentials. Therefore it is necessary to construct first a suitable effective interaction for such a limited space. We shall assume that it is a good approximation to treat the short-range correlations by solving the two-body scattering equation in the nuclear medium. In the Brueckner approximation this scattering equation is solved by treating the particle-particle scattering to all orders in an individual pair approximation [19]). The result of such a partial summation, known as the Brueckner G-matrix, is then a well-behaved interaction suitable for model spaces which span a range of single-particle energies up to 100 MeV. Although the interaction between the particles will have been properly renormalized for short-range correlations, the contributions due to short-range correlations to the self-energy still have to be considered explicitly. This means that their influence on the spectroscopic amplitudes is not included in our calculations. As discussed in the introduction this aspect can be well studied in nuclear

matter. Based on such studies [6,7]) and on the argument that the effect of short-range correlations will be largely independent of other aspects of nuclear structure, one expects that the short-range correlations remove 10–15% of the hole strength which appears then as particle strength at very high energy. This means that in the present results, which are obtained by including only excitations up to about 100 MeV from the Fermi energy, an overestimation of hole strength by roughly such an amount should be expected for orbitals which are occupied in mean field approximation.

In this work a G-matrix type of interaction is employed which is derived from an older version of the one-boson-exchange (OBE) potential [20]) of the Bonn group. Since the calculation of the G-matrix in finite nuclei is technically involved, it is convenient to calculate it in nuclear matter (NM). The resulting nuclear matter G-matrix is non-local and depends on the nuclear matter density (characterized by the Fermi-momentum k_F) and the starting energy. Because this energy dependence is weak, the nuclear matter G-matrix can be well approximated by calculating it only for an average starting energy [21,22]) (in the following denoted as E). The so-obtained G-matrix can then be represented by a local force [21]), which is parametrized as a set of meson-exchange potentials. It has been demonstrated that this simple effective force gives correctly the same binding energy and other quantities like Landau parameters in nuclear matter, as one obtains with the exact G-matrix [21]). It therefore contains all the features of the exact nuclear matter G-matrix and is simple enough to be manageable in nuclear-structure calculations. Its explicit form is:

$$G_{\mathrm{NM}}(q, E, k_F) = f_{E,k_F}(q) + f'_{E,k_F}(q)\tau_1 \cdot \tau_2 + g_{E,k_F}(q)\sigma_1 \cdot \sigma_2 + g'_{E,k_F}(q)\sigma_1 \cdot \sigma_2\tau_1 \cdot \tau_2 + h_{E,k_F}(q)S_{12}(q) + h'_{E,k_F}(q)S_{12}(q)\tau_1 \cdot \tau_2 , \tag{3.1}$$

with

$$S_{12}(q) = 3\sigma_1 \cdot q\sigma_2 \cdot q/q^2 - \sigma_1 \cdot \sigma_2 . \tag{3.2}$$

The functions f, f', etc. are sums of Yukawa interactions. The argument corresponds to the momentum the effective mesons carry. The essence of the G-matrix is thus contained in the q-dependence which is different for each spin-isospin operator. The form (3.1) facilitates the calculation of particle-hole matrix elements [see refs. [21,23,24])].

In this work two versions of this potential are employed. The first one is denoted by $G^{\mathrm{I}}_{\mathrm{NM}}$ and was calculated for nuclear matter with a Fermi momentum $k_F = 1.20\,\mathrm{fm}^{-1}$, which corresponds to 70% of the normal NM density, and an average starting energy $E = -74$ MeV. The second one is denoted by $G^{\mathrm{II}}_{\mathrm{NM}}$ and was calculated for nuclear matter with a Fermi momentum $k_F = 1.06\,\mathrm{fm}^{-1}$, which corresponds to 50% of the normal NM density, and an average starting energy $E = -20$ MeV. Due to the smaller density and starting energy the $G^{\mathrm{II}}_{\mathrm{NM}}$ interaction is somewhat stronger than the $G^{\mathrm{I}}_{\mathrm{NM}}$ interaction. However, it was shown in refs. [23,25]) that both interactions provided a reasonable approximation to a G-matrix, that was calculated for a finite

nucleus. Both interactions have been used before in nuclear structure calculations, providing good results [12,23,26-28,37]). The explicit parameters for both interactions can be found in the appendix.

No explicit density or energy dependence of the G-matrix interaction is considered here. It was shown in ref. [26]) that an explicit density dependence as used in a local density approximation is not necessary to obtain the correct surface properties for nuclear excitations. Therefore we make only this global correspondence between the density in nuclear matter and in finite nuclei. The neglect of the explicit energy dependence of the G-matrix has little influence on the results of the present work because the energy dependence is very weak, especially as compared to the energy dependence of the second-order self-energy.

The interactions $G^{\mathrm{I}}_{\mathrm{NM}}$ and $G^{\mathrm{II}}_{\mathrm{NM}}$ have been obtained with the conventional gap in the s.p. spectrum. Therefore they do not contain any detailed shell-structure information and consequently there is no essential double counting, provided that one includes only low-energy excitations in the intermediate summation of the 2p1h intermediate states in eq. (2.27). Naturally, one could avoid the problem of double counting completely by calculating the G-matrix for a particular nucleus with the consideration of only those two-particle intermediate states that lie outside the space one considers for the calculation of the self-energy.

We conclude that these interactions $G^{\mathrm{I}}_{\mathrm{NM}}$ and $G^{\mathrm{II}}_{\mathrm{NM}}$, though amenable to further improvements, should provide a suitable tool for the spectroscopic investigations presented here. This finds further support in the good results obtained in earlier spectroscopic calculations, especially of the fragmentation of the nuclear response [12]).

3.2. MODEL SPACE AND SINGLE-PARTICLE ENERGIES

The configuration space considered in the calculations is large enough to guarantee convergence for the excitations in the even–even nucleus [24,27,29]). This includes all shells below the Fermi surface and three major shells above. As single-particle states harmonic-oscillator wave functions with range parameters $b = 2.00$ fm for ^{48}Ca and $b = 2.12$ fm for ^{90}Zr were adopted.

For the s.p. energies around the Fermi energy experimental information on the energies of typical s.p. states in the adjacent odd nuclei was used. These states are characterized by large spectroscopic factors in one-nucleon transfer reactions and have therefore naively been interpreted as the original nucleus plus or minus one nucleon in a specific shell-model orbit. It is these states that we identify with the solutions of the Dyson equation with the largest spectroscopic factor and therefore it is these energies which were used in the expression for the self-energy (2.27). The shift of this quasiparticle energy with respect to the HF energy is almost entirely determined by the diagonal self-energy. So for the states around the Fermi energy one can obtain the corresponding "HF energy" uniquely by "undressing" the

empirical energy with the diagonal components of the self-energy (2.27):

$$\varepsilon_\alpha^{\mathrm{HF}} = \varepsilon_\alpha^{\mathrm{emp.}} - \Sigma^{(2)}_{\alpha\alpha}(\omega = \varepsilon_\alpha^{\mathrm{emp.}}) \,. \tag{3.3}$$

This procedure assures that for states around the Fermi energy the largest fragment of s.p. strength as solution of the Dyson equation coincides with the experimental information. The calculation then predicts the size of this fragment as well as the distribution and size of all the other fragments.

The empirical energies used are listed in table 1 for ^{48}Ca and for ^{90}Zr. Note that for ^{48}Ca the single-particle energies are similar to those given in ref. [30]) except for the proton gap which is 0.40 MeV larger and more in accordance with the binding energy of ^{47}K ($E_B = -400.118$ MeV) as quoted in ref. [31]). For hole orbits far from the Fermi energy such empirical information is mostly not available and the undressing procedure (3.3) loses its meaning because of the large fragmentation. Therefore we have taken these energies equal to the HF energies, assuming these may be considered as mean removal energies [17]) and provide a good characterization of the hole spectral functions. The same was done for the particle states far from the Fermi level. In this HF calculation the pure oscillator states were adopted instead of a fully self-consistent HF basis. Such a calculation provides s.p. energies with an energy spacing of $\hbar\omega \simeq 16$ MeV for ^{48}Ca and $\hbar\omega \simeq 14$ MeV for ^{90}Zr which is somewhat larger than the empirical harmonic-oscillator spacing $\hbar\omega = 41A^{-1/3}$ which is 11.28 MeV for ^{48}Ca and 9.14 MeV for ^{90}Zr. The more self-consistent HF single-particle states turned out to have a spacing of $\hbar\omega \simeq 24$ MeV for ^{48}Ca and $\hbar\omega \simeq 22$ MeV for ^{90}Zr, which we considered to be unrealistically large within the present approach.

Summarizing the procedure, we start with calculating a HF spectrum and replace the energies around the Fermi level by empirical energies. This set of energies is then used in the self-energy $\Sigma^{(2)}$ in eq. (2.27). The empirical energies are then undressed by relation (3.3) to obtain the corresponding HF single-particle energies.

TABLE 1

Quasiparticle energies ε in ^{48}Ca deduced from the neighboring nuclei ^{47}Ca, ^{49}Ca, ^{47}K, ^{49}Sc, and in ^{90}Zr deduced from the neighboring nuclei ^{89}Zr, ^{91}Zr, ^{89}Y, ^{91}Nb

^{48}Ca			^{90}Zr		
nl_j	ε_p	π_n	nl_j	ε_p	π_n
$1d_{3/2}$	−16.16	−12.52	$1f_{5/2}$	−10.11	−13.42
$2s_{1/2}$	−15.80	−12.54	$2p_{3/2}$	−9.87	−13.07
$1f_{7/2}$	−9.62	−9.94	$2p_{1/2}$	−8.36	−12.56
$2p_{3/2}$	−6.54	−5.14	$1g_{9/2}$	−5.16	−11.97
$1f_{5/2}$	−5.55	−1.14	$2d_{5/2}$	−3.20	−7.20
$2p_{1/2}$	−4.60	−3.12	$3s_{1/2}$	−1.00	−5.99
			$1g_{7/2}$	-	−5.32
			$2d_{3/2}$	-	−5.16

4. Hole spectral functions of ^{48}Ca

In the shell-model picture of ^{48}Ca the occupied proton states are the 2s1d shell, the 1p shell and, as the most deeply bound, the 1s shell. In the following we compare our calculated spectral functions with the most recently obtained (e, e'p) results [3]. The strengths are multiplied by $2j+1$ to indicate the relative yield of knocked-out protons and to facilitate a comparison with the sum rule value of $2j+1$ for completely filled orbits. For a comparison with experiment the spectral functions are represented in energy bins of 0.5 MeV.

4.1. THE $l=0$ SPECTRAL FUNCTION

In fig. 5 we compare the measured $l=0$ spectral function (upper part), which could be obtained up to 15 MeV excitation energy, with the calculated $l=0$ spectral function (lower part). Note that the first peak has been reduced by a factor five in this drawing.

The total occupancy of the $2s_{1/2}$ orbit in the ground state is calculated to be 1.73 (86%). The calculated $l=0$ strength up to 15 MeV is composed entirely of $2s_{1/2}$ strength and sums up to 1.58 (79% of the sum-rule value $2j+1$) which should be compared with the experimental value 1.39 (11) (69%). Above 15 MeV an additional 8% is therefore spread out over a large number (~400) of very small fragments up to 125 MeV, which corresponds to the energy of the highest 1p2h energy in the model space. The structures which show up around 20 MeV in the figure are already mainly composed of $1s_{1/2}$ strength.

Besides the global overestimation of the strength (~10%) in the experimentally probed region, it is also clear from the figure that in the calculation more strength should be shifted away from the ground state (1.52 calculated, versus 1.07 experimentally) to the first excited state, and that a stronger fragmentation mechanism is needed. Indeed such a stronger fragmentation is obtained by coupling the single-particle motion to collective particle-hole modes, e.g. in RPA, instead of to the uncorrelated particle-hole motion in fig. 2b [ref. [32])]. The total calculated strength within the experimentally analyzed energy range is not appreciably modified by such an extension, however.

4.2. THE $l=2$ SPECTRAL FUNCTION

The $l=2$ spectral function, shown in fig. 6, is the sum of the $1d_{3/2}$ and $1d_{5/2}$ spectral functions, which cannot be separated in the (e, e'p) experiment. Experimentally, the total strength observed up to 20 MeV amounts to 7.42 (63) (74% of the sum rule limit). The calculated strength up to 20 MeV is 7.98 (80%), which means there is a global overestimation of (6 ± 6)%.

The total calculated occupancy of the $1d_{3/2}$ orbit is 3.55 (89%) which is exhausted for a large part by the quasiparticle peak at 0.50 MeV excitation energy (with strength

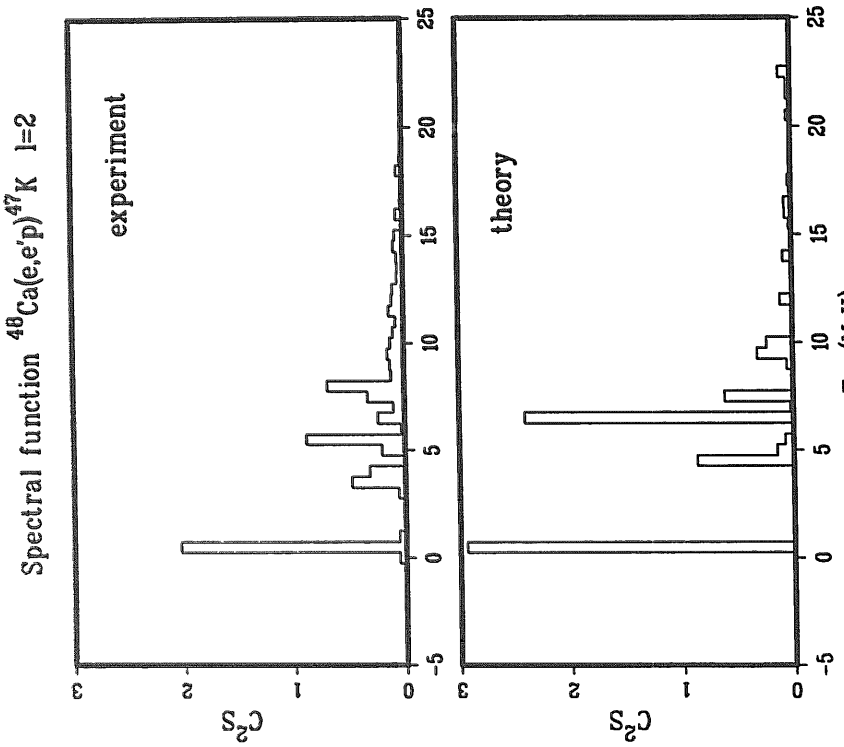

Fig. 6. The $l = 2$ spectral functions for ^{48}Ca.

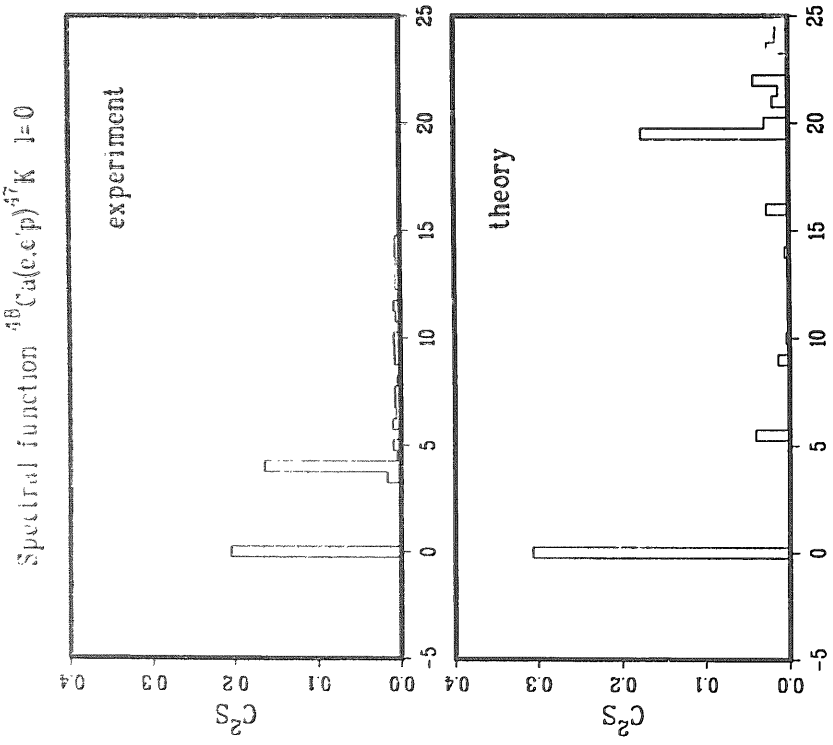

Fig. 5. The $l = 0$ proton spectral functions for ^{48}Ca. The state at $E_x = 0.0$ MeV has been multiplied by 0.2 for plotting purposes.

2.94 ~75%). The $1d_{3/2}$ spectral function has a similar behavior as the $2s_{1/2}$ spectral function. Besides the quasiparticle peak, which is overestimated by 25% of the sum rule, there are some obviously too weak states around 5 MeV and approximately 8% is spread over a large energy region (up to 125 MeV).

The total calculated occupancy of the $1d_{5/2}$ strength is 5.59 (93%) of which a large part is exhausted by the complex of states between 4 and 10 MeV (4.54 ~75%). In contrast with the $2s_{1/2}$ and $2d_{3/2}$ orbits, the $1d_{5/2}$ orbit is already strongly fragmented, although still fairly localized.

4.3. THE $l = 1$ SPECTRAL FUNCTION

The $l = 1$ spectral function is the sum of the $1p_{1/2}$ and $1p_{3/2}$ spectral functions. It was measured up to 23 MeV. As is seen from the upper part of fig. 7 the p-strength is clearly not saturated in the experimental region. The calculated $l = 1$ spectral function is shown in the lower part of fig. 7.

The strength is totally fragmented. The total spectral strength calculated in the region 0–23 MeV was 2.63 (44%), which should be compared to the experimental value 1.94 (24) (32%). The strength is overestimated by 12%, in line with the other hole spectral functions.

4.4. SUMMARY AND CONCLUSIONS

A first impression from figs. 5–7 is that the spreading of strength is rather similar in the calculation and in the data. This is a gratifying result in view of the very simple approximation (2.27) that was adopted for the self-energies. From a closer inspection of the figures one learns that indeed there are some systematic discrepancies between the calculations and the data which should be expected because of this simple self-energy approximation. The results are summarized in table 2, where occupation numbers are listed and the calculated strengths are compared with the observed strengths.

Firstly, the total calculated strength of the hole states is larger than the observed strength in the experimentally probed region by about 6–12% of the IPSM sum rule. This points in the direction of scattering of particles to very high energies by the strong short-range forces, which is not included in our calculation. The depletion of filled orbits due to this scattering is estimated in nuclear matter calculations to amount to 10–20% [refs. [6,7])]. This means that this strength is moved away from the hole spectral function to the particle spectral function and, if observable at all, should be found in transfer rather than knock-out reactions and at very high energies.

A second feature is the generally smoother distribution of strength in the data than calculated. One mechanism which would cause a finer fragmentation in the calculation was already indicated at the end of sect. 2, *viz.* a more self-consistent solution of the Dyson equation by substituting its solution back into the self-energy

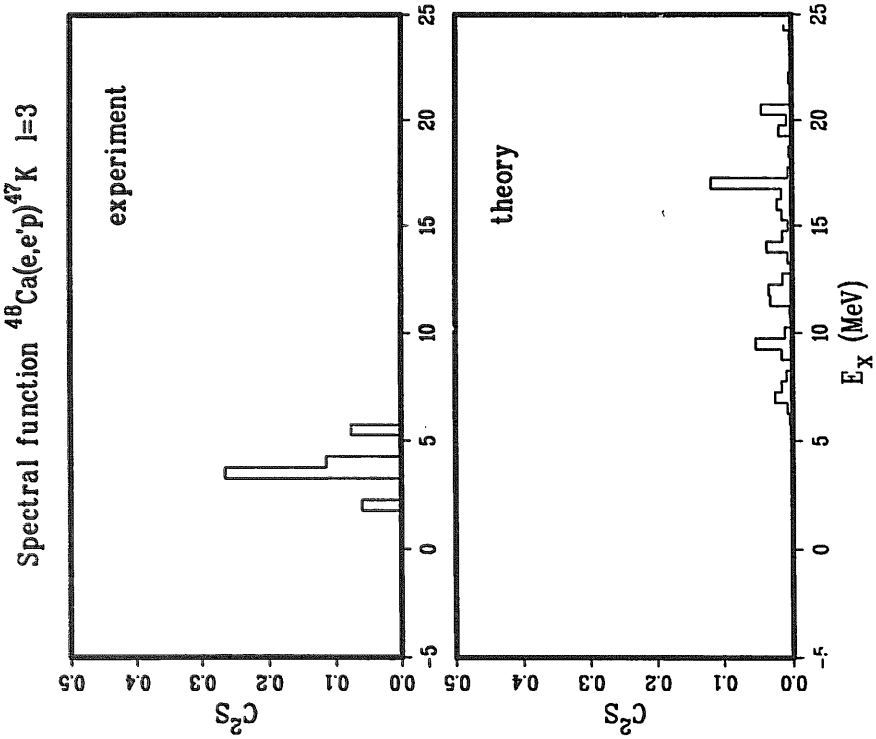

Fig. 8. The $l = 3$ spectral functions for ^{48}Ca.

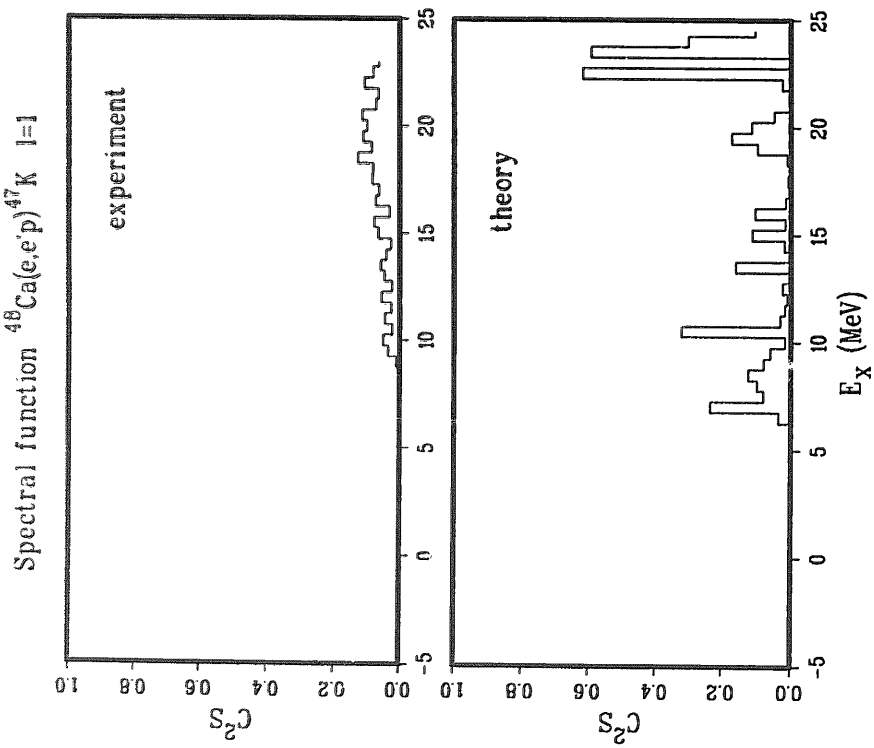

Fig. 7. The $l = 1$ spectral functions for ^{48}Ca.

TABLE 2

Occupation numbers and summed spectroscopic strengths for ^{48}Ca. The sum is taken over the experimental energy region (see text). The factor C^2 in the calculated results is $2j+1$

α	$n(\alpha)$	$\sum C^2S_l$ (calc)	$\sum C^2S_l$ (exp) [ref. [3]]
$1s_{1/2}$	0.97	-	-
$1p_{3/2}$	0.96	2.63	1.94 (24)
$1p_{1/2}$	0.95		
$1d_{5/2}$	0.93	7.98	7.42 (63)
$1d_{3/2}$	0.88		
$2s_{1/2}$	0.86	1.58	1.39 (11)
$1f_{7/2}$	0.07	0.29	0.51 (13)
$1f_{5/2}$	0.06		

and iterating until convergence is obtained [33]). This procedure would also ensure an exact conservation of particle number, which is now slightly violated. The total number of protons amounts to 20.05 and the total number of neutrons to 28.05, so this violation due to lack of complete self-consistency is only very small.

A third mechanism which would clearly improve the agreement between the calculation and the data is the coupling to correlated particle-hole states, e.g. the low-energy phonons. This would increase the size of the fragments about 5 MeV above the main peak through the coupling to the lowest 2^+, reducing the size of the quasiparticle peak [32]). This coupling to collective phonons is also of major influence on the $l=3$ strength shown in fig. 8. The experimentally observed strength below 5 MeV should be largely ascribed to the coupling of the $l=3$ strength to the self-energy terms with holes in the s- and d-shells coupled with the low-lying octupole state. The latter is not well represented in our calculation since the particle-hole pair is not correlated.

Having these three possible improvements of the theory in mind, we conclude that the results of the s, p and d shells are very satisfactory and encouraging.

5. Hole spectral functions of ^{90}Zr

In the IPSM picture of ^{90}Zr the occupied proton states are the 1f2p, 2s1d, 1p and 1s shells. However, ^{90}Zr cannot be considered as a "good" closed-shell nucleus like ^{48}Ca. Due to pairing correlations there is a non-negligible occupation of the proton $1g_{9/2}$ shell, and a considerable depletion of the 2p shells. In ref. [34]) these pairing correlations were treated in the broken-pair model, in a small model space and with a phenomenological interaction, leading to an occupation probability of 0.11 for the $1g_{9/2}$ and of 0.66 and 0.93 for the $2p_{1/2}$ and $2p_{3/2}$, respectively.

In view of this, one cannot expect a description of the proton spectral function for ^{90}Zr as good as for ^{48}Ca, using the self-energy (2.27). In this section we will

compare our calculated spectral functions for the hole states and for the 1g shells with those obtained in a recent (e, e'p) experiment [1]). The calculated spectral functions are represented in energy bins of 1 MeV to facilitate the comparison with experiment. All plotted results have been obtained with the G-matrix interaction G^{II}, which was also used for ^{48}Ca. With the slightly weaker interaction G^{I} only little different strength distributions were found. Therefore we present results with G^{I} only in table 3.

5.1. THE $l=1$ AND $l=4$ SPECTRAL FUNCTIONS

For the ^{90}Zr(e, e'p)^{89}Y reaction an l-decomposition has been performed up to 21 MeV [ref. [1])]. It was found that the $2p_{1/2}$, $2p_{3/2}$ and $1g_{9/2}$ strength was only located at low excitation energy ($E_x < 7$ MeV). The calculated $l=1$ spectral function (fig. 9) shows a completely similar picture: the $2p_{1/2}$ state at 0.0 MeV, the $2p_{3/2}$ state at 1.50 MeV and some weak states around 5 MeV. The total occupation of the $2p_{1/2}$ and $2p_{3/2}$ orbital in the ground state is 5.14 (86%). The total strength up to 21 MeV is 4.81 (80%). These numbers should be corrected for pairing correlations, however. If we make the crude approximation that the depletion caused by pairing correlations can be treated independently from the depletion caused by the coupling to 2p1h states then we can use the occupation numbers from ref. [34]) to calculate the spectroscopic strength including pairing correlations. This gives a total $l=1$ strength up to 21 MeV of 4.00 (67%), which still overestimates the data by 17% of the IPSM. From 21 MeV up to 150 MeV 5% is spread over a large number of very small states. This tail already starts at 7 MeV, but the solutions are so weak that they are not visible in the figure. The strength above 20 MeV is made up almost completely out of 1p strength.

The $l=4$ spectral function (fig. 10) shows clearly the effect of ground-state correlations for the valence states of ^{90}Zr. In the calculation, the strength up to 7 MeV is negligible (0.11). The strength up to 21 MeV is mainly $1g_{9/2}$ strength (0.48 for the $1g_{9/2}$ and 0.14 for the $1g_{7/2}$).

5.2. THE $l=3$ SPECTRAL FUNCTION

The effect of pairing correlations on the $1f_{5/2}$ and $1f_{7/2}$ states is much less, although still not negligible. In the broken pair calculation of ref. [34]) the occupation of these orbits was 0.97 and 0.98, respectively. In fig. 11 we compare our calculation with the experimental $l=3$ spectral function. The fragmentation of the calculated spectral function is very similar to that of the experimental one. The structure between 3.5 and 10 MeV is almost entirely $1f_{7/2}$ strength, while the strong state at 1.75 MeV is entirely $1f_{5/2}$. The $1f_{5/2}+1f_{7/2}$ strength up to 21 MeV is 11.39 (81%), which overestimates the experimental data by 17%. The total occupation of both orbits is 12.85 (92%), which means that 11% is found above 21 MeV. The fragmentation of these

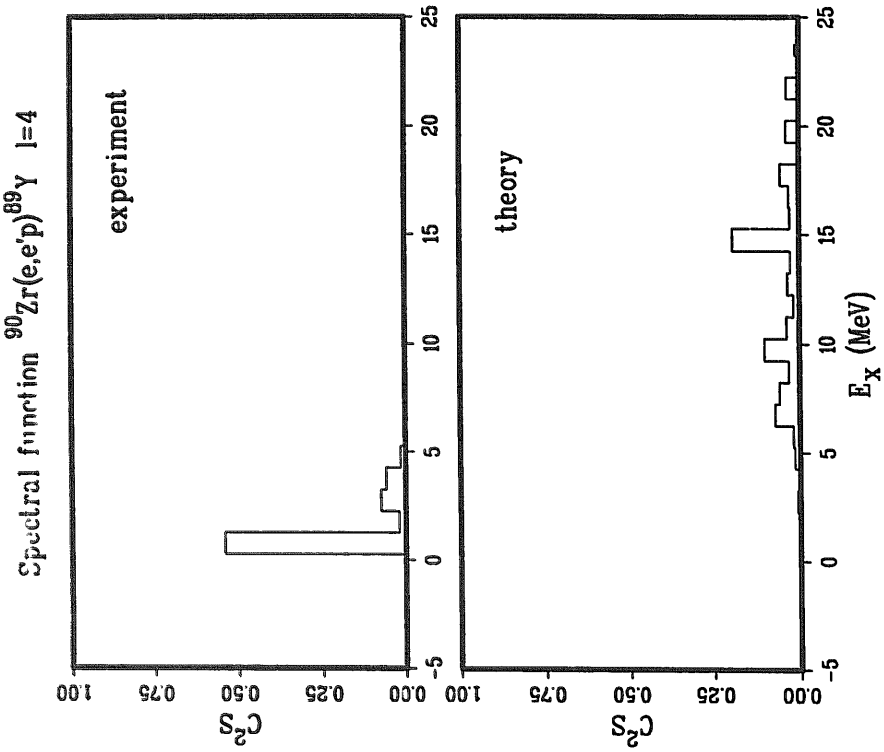

Fig. 10. The $l = 4$ spectral functions for ^{90}Zr.

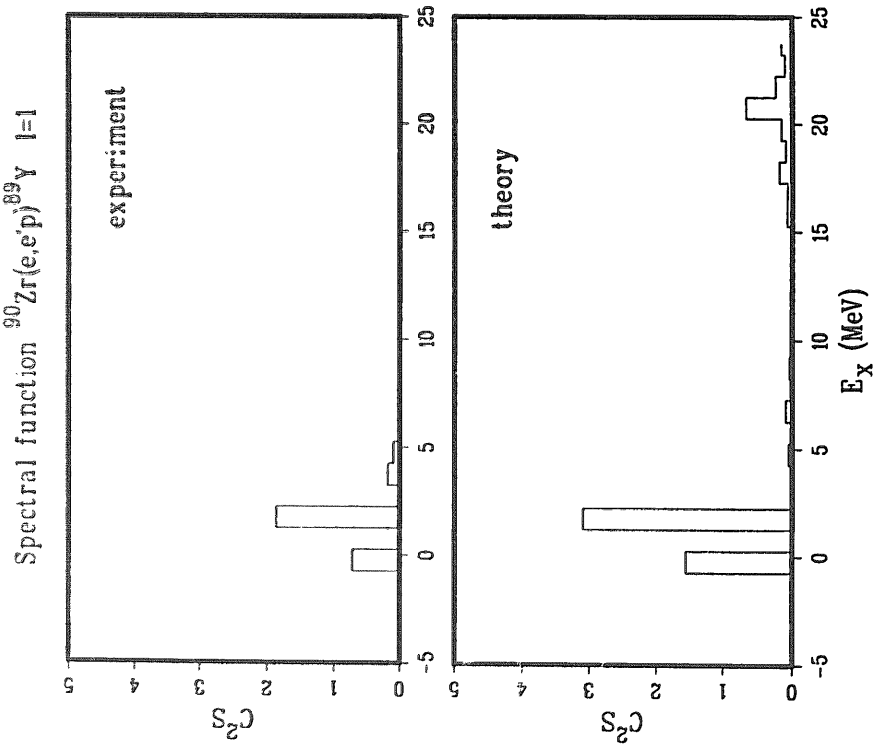

Fig. 9. The $l = 1$ spectral functions for ^{90}Zr.

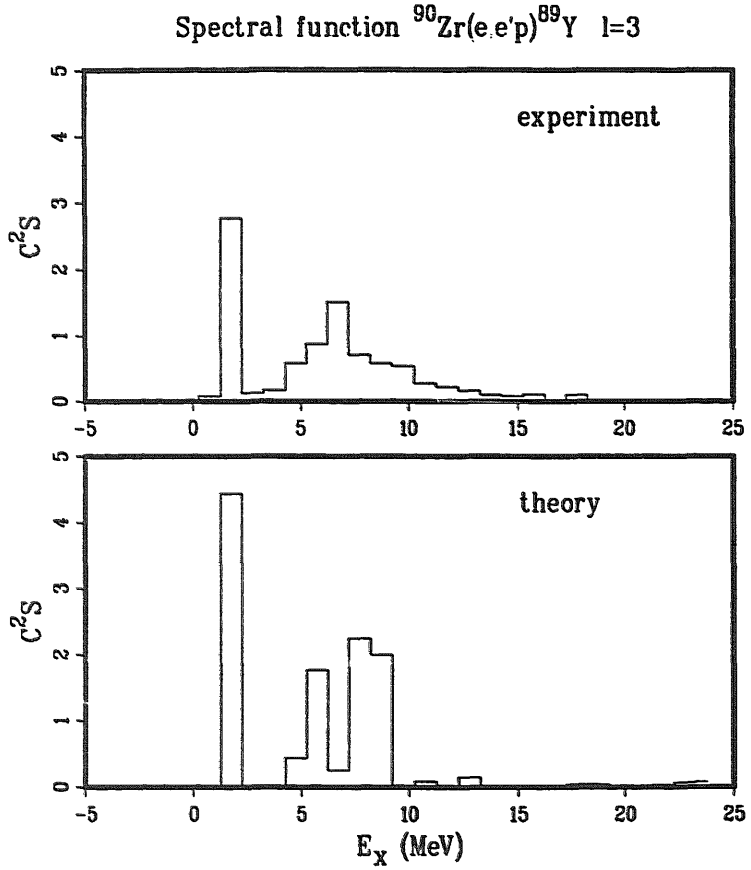

Fig. 11. The $l=3$ spectral functions for ^{90}Zr.

orbitals is very similar to the $1d_{3/2}$ and $1d_{5/2}$ orbitals in ^{48}Ca. Inclusion of pairing correlations gives a total strength of 11.08 (79%), which exceeds the data by 17% of the IPSM sum rule.

5.3. THE $l=2$ AND $l=0$ SPECTRAL FUNCTION

The $l=2$ (fig. 12) and $l=0$ (fig. 13) spectral functions have in common, that their strength is not saturated in the experimental region. For both spectral functions the fragmentation of the experimental and calculated functions is very similar. The total spectral strength up to 21 MeV is for the $l=2$ function $(1d_{3/2}+1d_{5/2})$ 6.36 (64%) and for the $l=0$ function 1.41 (71%), which exceed the experimental values by 19% and 20% respectively of the IPSM sum rule.

5.4. SUMMARY AND CONCLUSIONS

In table 3 we summarize the calculated occupation numbers of the hole states and the 1g states and the summed spectroscopic strengths up to 21 MeV. To complete the list of occupation probabilities we mention those here for the interaction G^{II}. We obtained for $1s_{1/2}$: 0.98, $1p_{3/2}$: 0.97, $1p_{1/2}$: 0.97 and for the higher orbits $2d_{5/2}$:

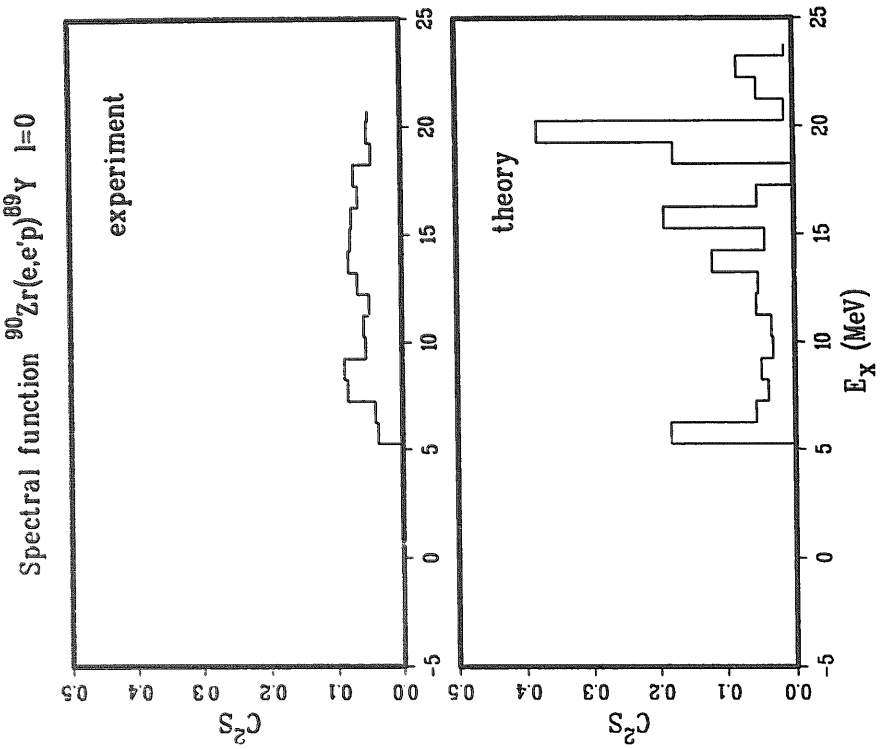

Fig. 13. The $l = 0$ spectral functions for ^{90}Zr.

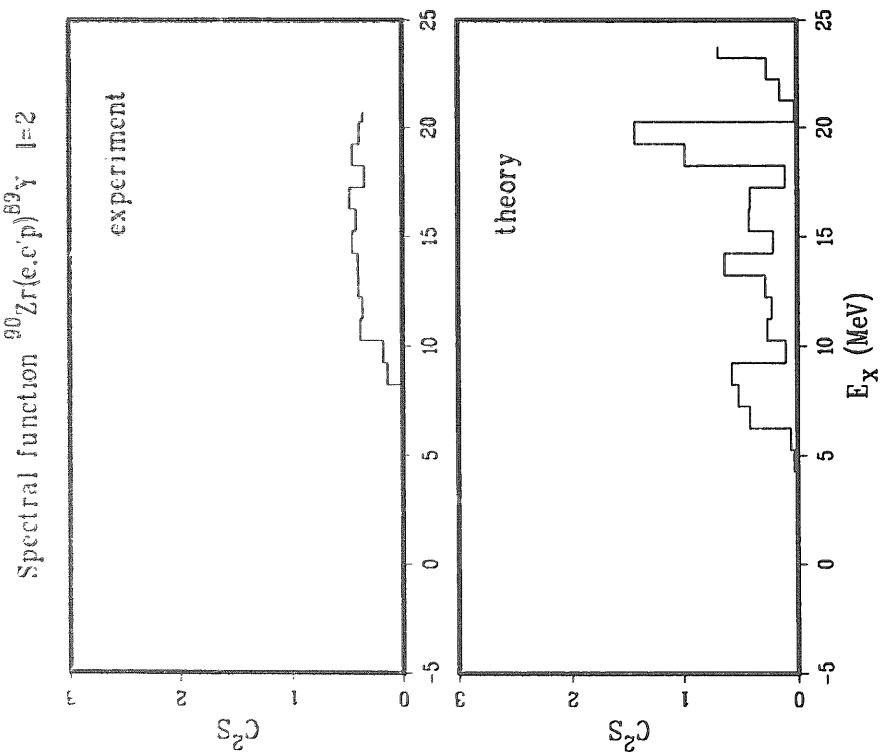

Fig. 12. The $l = 2$ spectral functions for ^{90}Zr.

TABLE 3

Occupation numbers and summed spectroscopic strengths for ^{90}Zr. The sum is taken over the experimental energy region (0-21 MeV). The factor C^2 in the calculations is $2j+1$

α	$n(\alpha)$		$\sum C^2S_l$(calc)		$\sum C^2S_l$ (exp) [ref. [1])]
	G^{I}	G^{II}	G^{I}	G^{II}	
$1d_{5/2}$	0.97	0.96	6.54	6.36	4.51 (38)
$1d_{3/2}$	0.96	0.95			
$2s_{1/2}$	0.97	0.96	1.45	1.41	1.02 (6)
$1f_{7/2}$	0.94	0.93	11.84	11.39	8.75 (63)
$1f_{5/2}$	0.91	0.90	11.52 [a])	11.08 [a])	
$2p_{3/2}$	0.90	0.88	5.03	4.81	2.97 (15)
$2p_{1/2}$	0.88	0.86	4.20 [a])	4.00 [a])	
$1g_{9/2}$	0.08	0.08	0.62	0.69	0.69 (12)
$1g_{7/2}$	0.04	0.04	0.11 [b])	0.11 [b])	

[a]) Including pairing correlations (see text).
[b]) Spectroscopic strength up to 7 MeV.

0.054, $2d_{3/2}$: 0.041, $3s_{1/2}$: 0.038. For still higher orbits the occupation probability is less than 2%. Comparing the results for ^{90}Zr with those for ^{48}Ca one can draw similar conclusions as in sect. 4. The calculations for the deep-lying hole states seem to indicate that a quenching of 15-20% through short-range or other not yet included correlations is needed for ^{90}Zr, which is larger than for ^{48}Ca. A possible partial explanation for this larger discrepancy may be that Coulomb distortions of the electron wave function were not yet fully included in the analysis of the data [1]). This might increase the experimental numbers by some 5% [ref. [35])]. Other reasons for the larger discrepancy may be found in various aspects of the calculations. For the valence orbits the picture is obscured somewhat by pairing correlations, which already lead to a considerable depletion of the p-shells. Moreover, without pairing correlations the low-lying 2^+ in ^{90}Zr is absent and hence the fragmentation by coupling to this state is also missing in our calculations. We do not expect that the larger discrepancy for ^{90}Zr than for ^{48}Ca may be due to the limitation of the model space, because six major shells were included for ^{48}Ca and seven major shells for ^{90}Zr.

6. Quasiparticle approximation and optical potential

The spectral functions describing the single-particle strength below the Fermi energy, can also be analyzed in terms of the quasiparticle approximation. For single-particle strength above the Fermi energy this analysis is usually related to the empirical optical potential deduced from elastic nucleon-nucleus scattering. This subject has been extensively reviewed recently by Mahaux *et al.* [36]). A problem in comparing the self-energy [eq. (2.27)] directly with the optical potential is its

singular behavior as a function of energy. The empirical optical potential, on the other hand, is a smooth function of energy, which can be obtained from the self-energy by a suitable energy-averaging procedure [36]). It is also usually given as a local potential in coordinate space. Note that in the coordinate representation the self-energy used in this work [eq. (2.27)] is non-local. Another problem is that the empirical optical potential is used as an irreducible interaction with respect to the propagation of a plane wave particle. In the present paper, the self-energy is irreducible with respect to the propagation of a Hartree-Fock particle or hole. A comparison can therefore strictly only be made for the reducible interactions which can be related to the cross sections. This is beyond the scope of the present paper.

In earlier work (refs. [13-15])) related to the study of the removal of protons, the imaginary part of the self-energy was studied as in eq. (2.27). Only the first part of eq. (2.27) was considered, however, which results in zero depletion of occupied orbitals. The 1p2h contributions to the imaginary part of the self-energy appear as narrow peaks on a continuous background in refs. [14,15]) due to the use of continuum wave functions for particle states. As such these contributions are very similar to the delta-function contributions at the 2p1h and 1p2h energies in eq. (2.27) when a discrete basis is used. These calculations were feasible due to the use of simple zero-range interactions and were only carried out for light nuclei like ^{16}O. The calculated imaginary part of the optical potential reached values of 5–10 MeV for separation energies of 40 MeV and higher. Below this energy the spectral functions were found to consist of small peaks with widths typically less than 0.5 MeV.

In several more recent studies of the optical potential using more realistic G-matrix interactions a similar size and energy dependence of the imaginary part of the optical potential has been obtained for scattering states [37]). As discussed above, it is not the aim of the present work to construct the optical potential. For the real part this would not be meaningful since empirical single-particle energies have been adopted.

In order to make contact with empirical determinations of the strength of the imaginary part of the optical potential a comparison at the level of the quasiparticle approximation to the spectral function will be considered:

$$S_\alpha^{\mathrm{QP}}(\omega) = \frac{1}{\pi} z_\alpha \frac{\frac{1}{2}\Gamma_\alpha}{(\omega - E_\alpha)^2 + (\frac{1}{2}\Gamma_\alpha)^2} . \tag{6.1}$$

Here, z_α is the total strength contained in this distribution, which in a homogeneous system can be directly related to the derivative with respect to energy of the real part of the self-energy at the quasiparticle energy E_α which describes the position of the peak. The width Γ_α is related to the imaginary part of the self-energy by

$$\Gamma_\alpha = 2 z_\alpha \, \mathrm{Im} \, \Sigma_{\alpha\alpha}(E_\alpha) . \tag{6.2}$$

Taking this result too literally in finite nuclei is not useful when a discrete basis is used as is the case in this work. Nevertheless, it is clear that the distribution of single-particle strength for a given orbital as obtained in this work, can be interpreted

in terms of a width when the strength is fragmented as is the case for orbitals not in the immediate vicinity of the Fermi energy. That such a concentration in quasiparticle "peaks" or "bumps" does indeed occur is illustrated in fig. 14, where the calculated s-strength for ^{48}Ca is displayed. In this figure the s.p. strength is shown differently from the preceding figures of the spectral functions. In fig. 14 both the hole and the particle domain are covered, with the most deeply bound strength on the left. The s.p. strength crosses the Fermi energies at −15.80 MeV (the large peak in the figure corresponding to ε_F^- and −9.62 MeV (ε_F^+) at which point it must be referred to as particle strength. In the figure a smearing procedure with a width of 1 MeV has been applied. The resulting strength distributions can then be interpreted according to eq. (6.1), allowing the extraction of a width the value of which is compared to empirical results available in the literature [38-40]). The smearing width is not included in this comparison. For orbitals which have a very large portion of their strength concentrated in a single peak it is obviously appropriate to adopt a zero width. Strength not contained in the quasiparticle peak is usually referred to as background strength. In addition to this background, there is strength located on the other side of the Fermi energy where there is no quasiparticle peak.

The results shown in fig. 14 indicate that the spectral functions which are obtained with this procedure are not exactly represented by a lorentzian [see eq. (6.1)]. This is natural since the amount of phase space corresponding to 2p1h and 1p2h states increases with increasing distance from the Fermi energy. As a result an inevitable asymmetry in the peak structure will develop for orbitals which are not too close to the Fermi energy. Especially for the $1s_{1/2}$ it is somewhat arbitrary to assign a

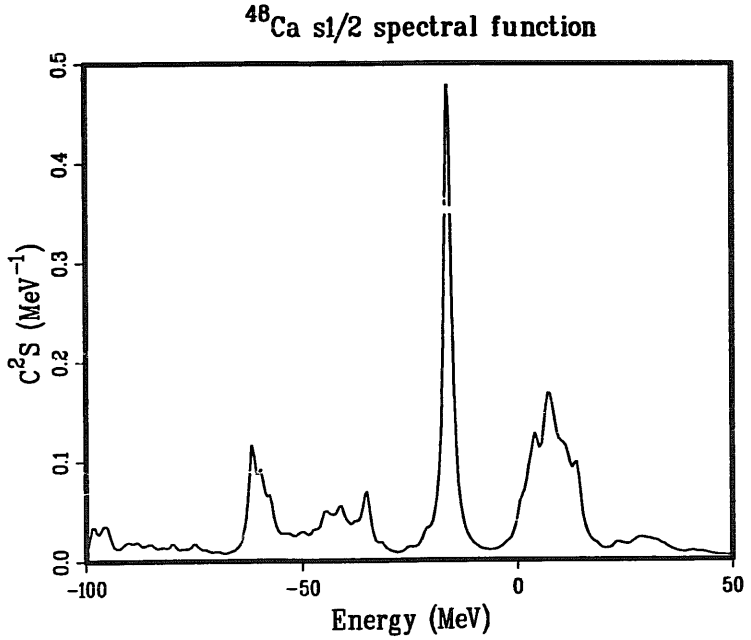

Fig. 14. The full $s_{1/2}$ spectral function of ^{48}Ca. To obtain a continuous distribution all solutions are dressed with a small width (1.0 MeV).

quasiparticle peak between −70 and −30 MeV with a corresponding width $\Gamma \simeq$ 20 MeV. However, for all other orbitals a meaningful extraction of a width can be obtained as for instance in the case of the $3s_{1/2}$ orbital shown in fig. 14. A quasiparticle energy of 10 MeV with a width of 11 MeV can be unambiguously extracted.

The resulting widths that are obtained with this procedure are displayed in fig. 15 for the proton orbits in ^{48}Ca and for ^{90}Zr. These widths (dots in the figure) are plotted as a function of energy distance to the Fermi energy and can be compared with three analytical expressions found in the literature. Brown and Rho [38]) deduced from ref. [41]) the following expression

$$\tfrac{1}{2}\Gamma^{\mathrm{BR}}(\omega) = \frac{12(\omega-\varepsilon_{\mathrm{F}})^2}{(\omega-\varepsilon_{\mathrm{F}})^2+500}\ \mathrm{MeV} \tag{6.3}$$

which at small $\omega - \varepsilon_{\mathrm{F}}$ has the characteristic quadratic dependence found in infinite Fermi systems. An alternative expression was suggested by Jeukenne and Mahaux [39])

$$\tfrac{1}{2}\Gamma^{\mathrm{JM}}(\omega) = \frac{9(\omega-\varepsilon_{\mathrm{F}})^4}{(\omega-\varepsilon_{\mathrm{F}})^4+13.27^4}\ \mathrm{MeV} \tag{6.4}$$

based on the argument that in a finite nucleus the level density and therefore also the width near the Fermi energy is reduced as compared to infinite systems. A third expression, also based on the work in ref. [41]), was used by Smith and Wambach [40]) in a study of the nuclear response. It reads

$$\tfrac{1}{2}\Gamma^{\mathrm{MN}}(\omega) = \frac{10.75(\omega-\varepsilon_{\mathrm{F}})^2}{(\omega-\varepsilon_{\mathrm{F}})^2+18^2}\,\frac{110^2}{110^2+(\omega-\varepsilon_{\mathrm{F}})^2}\ \mathrm{MeV}\,. \tag{6.5}$$

The results deduced from the spectral functions agree very well with these empirical parametrizations. Especially for states below the Fermi energy, they are very well represented by eq. (6.3). This confirms once again the encouraging results that have been obtained for the strength distributions in comparison with the (e, e'p) results. For the states above 20 MeV (relative to ε_{F}) in the particle domain, the widths are smaller than the empirical curves, in particular for ^{90}Zr. A calculation of the self-energy with continuum wave functions might lead to improved results. In addition, a limited set of oscillator states has been used in the present work. One must also keep in mind that eq. (2.27) provides only the lowest order process that can contribute to the width. Substitution of the obtained Green functions back into the calculation of the self-energies may also increase the widths [42]). Nevertheless, it seems that one can already account for most of the observed widths and therefore the imaginary parts of the optical potential at low energy.

It is possible to use eq. (6.1) for an estimate of the strength in the background (i.e. not under the peak) when the orbitals are close to the Fermi energy. This can be done by subtracting z_α from the amount of occupation ($n(\alpha)$) or depletion ($1-n(\alpha)$) (see e.g. tables 2 and 3). The resulting background contribution is typically

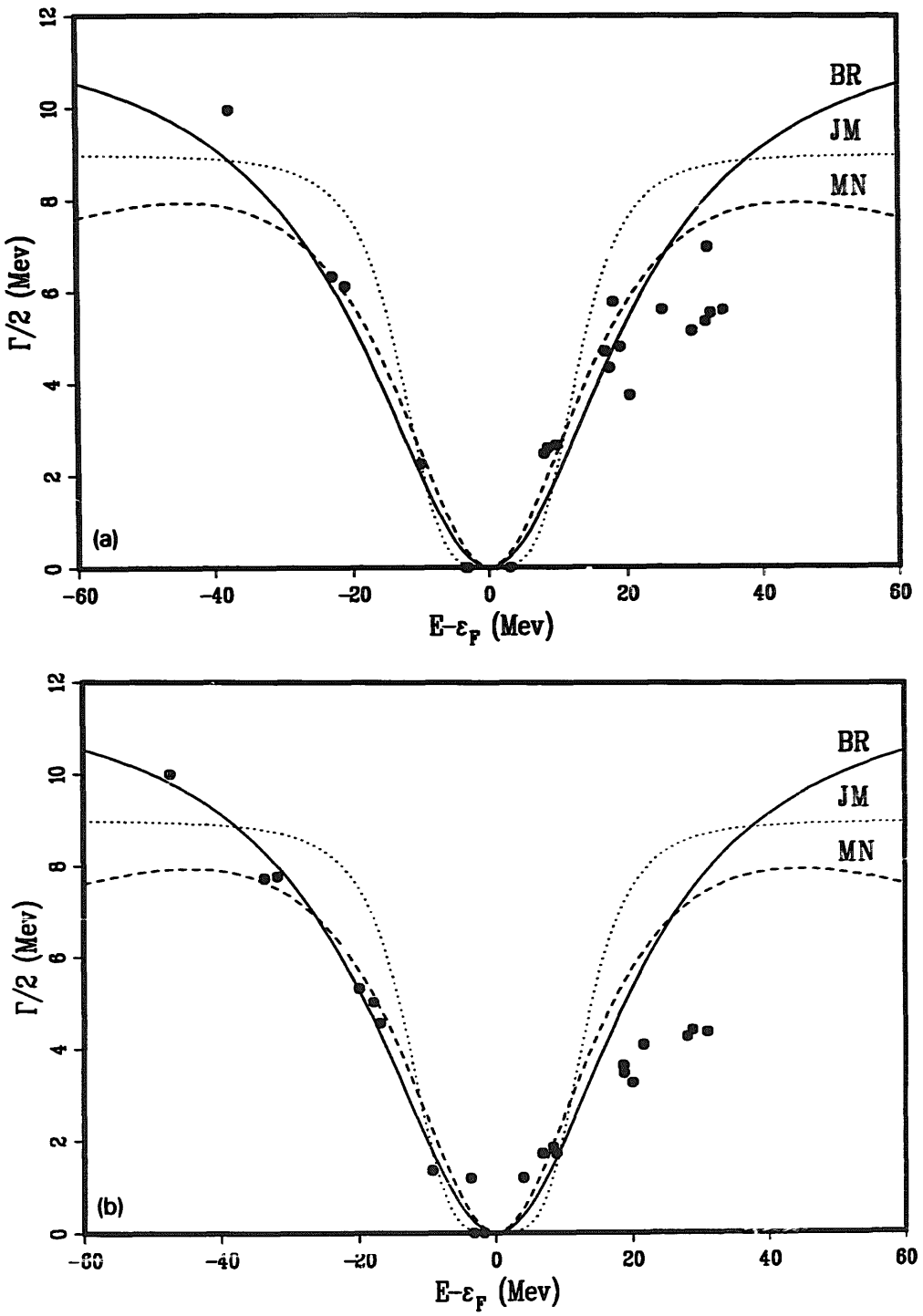

Fig. 15. Widths of the quasiparticle peaks for proton orbitals in ^{48}Ca (upper figure) and ^{90}Zr (lower figure) obtained from the calculated strength distributions as described in the text. The three curves in the figure represent the empirical parametrizations given by eqs. (6.3)-(6.5). The Fermi energy ε_F is the average of the Fermi energies ε_F^+ and ε_F^-.

of the order of 10%. Such results are also obtained in calculations of the hole part of the spectral function in nuclear matter [see e.g. refs. [7,43])] when realistic interactions are used. Although it is expected that the total amount of strength for mean field orbitals below the Fermi energy will be further reduced by about 10–15% when short-range and tensor correlations are fully incorporated, it is clear that a background contribution of about 10% emerges from most theoretical investigations [see refs. [7,43,44]) and this work].

7. Spectral functions and the validity of the shell model

In the preceding sections only results for proton removal were discussed and compared to experiment. The results for neutrons are naturally very similar and not discussed here, as it was our aim to focus on the comparison with the newly available data for proton knock-out using the (e, e'p) reaction. It is also important to note that we have concentrated on the discussion of the distribution of spectroscopic strength and have foregone any comparisons of momentum distributions related to individual transitions. No effort has been made to optimize the description of these momentum distributions by using a basis (e.g. of Woods–Saxon states) which yields a good correspondence with the experimental momentum distributions. The reason is that in structure calculations a Woods–Saxon or harmonic-oscillator basis have been found to yield similar results [45]). Because this work focuses on the general features of the strength distribution, the technically easier to handle oscillator basis with reasonable range parameters has been chosen.

Other theoretical results for occupation numbers usually refer to ^{208}Pb. Using an analysis based on the dispersion relation which connects the real part of the self-energy with the imaginary part, it is possible to relate this imaginary part with empirical optical potentials [44]). Making the assumption that the imaginary part of the self-energy is symmetrical around the Fermi energy these authors obtain results for spectroscopic factors and occupation probabilities for states just below the Fermi energy of 0.66 and 0.77, respectively. In the work of ref. [44]) the asymmetry which exists between the 2p1h and 1p2h phase space, especially with regard to short-range correlations [6,7]) is not taken into account. It is also not possible to study the energy dependence of the fragmentation of the orbitals away from the Fermi energy as it has been shown here. Nevertheless, the results of ref. [44]) are in good agreement with the most recent analysis of the (e, e'p) experiment on ^{208}Pb in which Coulomb distortion was properly taken into account [35]). In agreement with the present work the additional background distribution in $A-1$ system is found to contain only about 10% of the IPSM sum rule.

As is shown here, it is important to calculate the influence of low-energy excitations in the finite system itself. It seems therefore that a consistent picture of the depletion of shell-model orbitals is emerging. From the present work one can infer that a 10% background contribution to the hole strength is indeed a reasonable estimate. By

subtracting an additional 10–15% from the calculated occupation numbers on account of short-range correlations, one arrives at numbers which are quite similar to what is obtained from the direct analysis of the (e, e'p) experiments as well as in a combined analysis with (e, e') elastic scattering data [46]).

The spectral functions shown in sects. 4 and 5 exhibit a quite general characteristic feature. This is that the fragmentation of strength and the width of the range over which this strength is distributed increases with increasing distance from the Fermi energy. States lying close to the Fermi level, called "valence" shells in the shell model, still have a strong peak which carries the main portion of the strength, i.e. typically 50% or more of the sum rule value $2j+1$. This "quasiparticle" state is what is observed experimentally in the $A-1$ nucleus and interpreted in the naive shell model as a single-hole state (and similarly for single-particle states in the $A+1$ system). Hole states or particle states which are remote from the Fermi level are in the same region where 1p2h or 2p1h states, respectively, are abundantly present, with which they mix by means of the coupling through the interaction. Thereby these states spread over a broad energy region and one can distinguish a "quasiparticle bump" as was illutrated by fig. 14. The width of the deep-lying bump, mainly composed of 1s strength, is so large that the notion of a nucleon orbit loses its meaning. In view of this the question arises how the shell model can still be meaningful for the valence orbits. The answer is obvious that their quasiparticle energies are far enough away from the 1p2h or 2p1h energies. This can only happen because there is a finite gap in the single-particle spectrum, which has obviously to do with the finite size of the nucleus. The larger the nucleus the smaller this gap and consequently the stronger the reduction of the "quasiparticle" strength in the main peak.

These results are in clear contrast with a mean field picture. For instance for the shells of an atomic electron cloud the HF approximation works very well; all hole states have a well-defined energy and the quasiparticle peak contains virtually 100% of the strength. The nucleus has an intermediate structure between the atom and a quantum liquid like ^{3}He for which the quasiparticle peak at the Fermi surface is at most 30% [ref. [47])] and must be considered a more strongly correlated system. This means that nuclear matter should really be considered as a quantum liquid rather than an assembly of particles moving almost independently in orbits of the size of the nuclear diameter. It may be remarked that there is also a similarity as far as interactions are concerned. A Lennard-Jones potential also has a strong repulsive core and a longer range attraction. There is even a further analogy when this repulsive core is attributed to Pauli repulsion of the constituents (electrons in the case of the atom and quarks in the case of nucleons). The difference between a nucleus and a liquid ^{3}He is of course the finite size, which yields the aforementioned gap in the s.p. spectrum and therefore increases the range of validity of the quasiparticle (shell-model) picture. One can conclude nevertheless that the nuclear shell model reveals a quasiparticle picture which is very similar to the one developed by Landau

for strongly interacting Fermi liquids [48]). Further discussion of these features including the influence of short-range correlations on the strength distributions can be found in refs. [49,50]).

We would like to thank G.J. Kramer for providing us with the (e, e'p) data prior to publication.

Appendix

PARAMETERS OF THE G-MATRIX INTERACTION

The local parametrization of the G-matrix of the Bonn potential [21]) used in this work consists of two parts:

$$G = V + \tilde{G}, \tag{A.1}$$

in which V represents the bare nucleon-nucleon interaction and $\tilde{G}$ the (nuclear matter) G-matrix correlations. In the G-matrix interaction of ref. [21]) an older version of the Bonn potential [20]) was used as bare interaction. This potential is parametrized as a set of one-boson exchange potentials, using the spin-isospin operators $\mathbf{1}$, $\boldsymbol{\tau}_1 \cdot \boldsymbol{\tau}_2$, $\boldsymbol{\sigma}_1 \cdot \boldsymbol{\sigma}_2$ and $\boldsymbol{\sigma}_1 \cdot \boldsymbol{\sigma}_2 \boldsymbol{\tau}_1 \cdot \boldsymbol{\tau}_2$ to represent the central part and S_{12} and $S_{12}\boldsymbol{\tau}_1 \cdot \boldsymbol{\tau}_2$ to represent the tensor part ($S_{12}(\boldsymbol{q}) = 3\boldsymbol{\sigma}_1 \cdot \hat{\boldsymbol{q}} \boldsymbol{\sigma}_2 \cdot \hat{\boldsymbol{q}} - \boldsymbol{\sigma}_1 \cdot \boldsymbol{\sigma}_2$). For instance the one-pion-exchange (OPE) potential is written as:

$$\begin{aligned} V_\pi(\boldsymbol{q}) &= \frac{-f_\pi^2}{m_\pi^2} \frac{\boldsymbol{\sigma}_1 \cdot \boldsymbol{q} \boldsymbol{\sigma}_2 \cdot \boldsymbol{q}}{m_\pi^2 + q^2} \boldsymbol{\tau}_1 \cdot \boldsymbol{\tau}_2 \\ &= C_\pi \frac{q^2}{m_\pi^2 + q^2} S_{12}(\boldsymbol{q}) \boldsymbol{\tau}_1 \cdot \boldsymbol{\tau}_2 + C_\pi \frac{q^2}{m_\pi^2 + q^2} \boldsymbol{\sigma}_1 \cdot \boldsymbol{\sigma}_2 \boldsymbol{\tau}_1 \cdot \boldsymbol{\tau}_2 . \end{aligned} \tag{A.2}$$

The nuclear matter G-matrix correlations are dependent on the average starting energy E and Fermi momentum k_F (see sect. 3.1). The central parts of these G-matrix correlations are parametrized [21]) as a set of Yukawa potentials

$$\sum_j C_j \frac{1}{m_j^2 + q^2} \times \text{spin-isospin operator}, \tag{A.3}$$

while the tensor parts are parametrized as:

$$\sum_j C_j \frac{q^2}{m_j^2 + q^2} S_{12}(\boldsymbol{q}) \times \text{isospin operator}. \tag{A.4}$$

In these expressions m_j represents the mass of an exchanged meson and C_j the strength. The total nuclear matter G-matrix interaction is therefore parmetrized as:

$$\begin{aligned} G_{\mathrm{NM}}(\boldsymbol{q}, E, k_F) = {} & f_{E,k_F}(\boldsymbol{q}) + f'_{E,k_F}(\boldsymbol{q}) \boldsymbol{\tau}_1 \cdot \boldsymbol{\tau}_2 + g_{E,k_F}(\boldsymbol{q}) \boldsymbol{\sigma}_1 \cdot \boldsymbol{\sigma}_2 + g'_{E,k_F}(\boldsymbol{q}) \boldsymbol{\sigma}_1 \cdot \boldsymbol{\sigma}_2 \boldsymbol{\tau}_1 \cdot \boldsymbol{\tau}_2 \\ & + h_{E,k_F}(\boldsymbol{q}) S_{12}(\boldsymbol{q}) + h'_{E,k_F}(\boldsymbol{q}) S_{12}(\boldsymbol{q}) \boldsymbol{\tau}_1 \cdot \boldsymbol{\tau}_2 , \end{aligned} \tag{A.5}$$

TABLE 4

Parameters for the used interactions

	G^{I}_{NM}			G^{II}_{NM}		
Symmetry	C	m (MeV)	λ	C	m (MeV)	λ
1	−59.345	500	0	−59.345	500	0
	−22.347	600	0	−31.245	575	0
	353.35	850	0	353.35	850	0
	−633.71	1500	0	−633.71	1500	0
	−228.74	1550	0	−146.35	1600	0
$\tau_1 \cdot \tau_2$	22.536	700	0	22.536	700	0
	34.432	725	0	27.691	625	0
	−130.07	1200	0	−130.07	1200	0
	−119.37	1500	0	−108.43	1500	0
$\sigma_1 \cdot \sigma_2$	−0.7546	725	2	−0.7546	725	2
	−24.294	800	0	−14.86	650	0
	−1.6975	810	2	−1.6975	810	2
$\sigma_1 \cdot \sigma_2 \tau_1 \cdot \tau_2$	−0.6077	138.50	2	−0.6077	138.50	2
	−1.3046	590	2	−1.3046	590	2
	1.2993	475	0	1.9187	450	0
S_{12}	−0.7546	725	2	−0.7546	725	2
	0.8487	810	2	0.8487	810	2
	0.6597	1750	2	2.148	3000	2
$S_{12}\tau_1 \cdot \tau_2$	−0.6077	138.50	2	−0.6077	138.50	2
	0.6523	590	2	0.6523	590	2
	0.0059	450	2			

in which the functions f, f', etc, are given by

$$f(q)=\sum_j \frac{C_j q^{\lambda_j}}{m_j^2+q^2} \qquad \lambda_j=0 \text{ or } 2\,. \tag{A.6}$$

We use two versions of this potential. The first one is denoted by G^{I}_{NM} and was calculated for $k_F=1.20\,\mathrm{fm}^{-1}$ and $E=-74$ MeV. The second one is denoted by G^{II}_{NM} and was calculated for $k_F=1.06\,\mathrm{fm}^{-1}$ and $E=-20$ MeV. The parameters for these interactions were taken from refs. [21,23]) and are summarized in table 4.

References

1) J.W.A. den Herder, H.P. Blok, E. Jans, P.H.M. Keizer, L. Lapikas, E.N.M. Quint, G. van der Steenhoven and P.K.A. de Witt Huberts, Nucl. Phys. **A490** (1988) 507
2) E.N.M. Quint, Ph.D. thesis, NIKHEF, Amsterdam (1988)
3) G.J. Kramer, Ph.D. thesis, NIKHEF, Amsterdam (1990)
4) P.K.A. de Witt Huberts, J. of Phys. **G16** (1990) 507
5) V.R. Pandharipande, C.N. Papanicolas and J. Wambach, Phys. Rev. Lett. **53** (1984) 1133
6) A. Ramos, A. Polls and W.H. Dickhoff, Nucl. Phys. **A503** (1989) 1
7) O. Benhar, A. Fabrocini and S. Fantoni, Nucl. Phys. **A503** (1989) 375

8) B.H. Brandow, Phys. Rev. **152** (1966) 853
9) B.D. Day, Phys. Rev. **C24** (1981) 1203
10) W.J. McDonald, R.N. MacDonald, W.C. Olsen, R. Dymarz, F. Khanna, L. Antonuk, J.M. Cameron, P. Kitching, G.C. Neilson, D.M. Sheppard, D.A. Hutcheon, C.A. Miller and J. Kallne, Nucl. Phys. **A456** (1986) 577
11) J. Mougey, Nucl. Phys. **A335** (1980) 35
12) M.G.E. Brand, K. Allaart and W.H. Dickhoff, Nucl. Phys. **A509** (1990) 1
13) D.H.E. Gross and R. Lipperheide, Nucl. Phys. **A150** (1970) 449
14) U. Wille and R. Lipperheide, Nucl. Phys. **A189** (1972) 113
15) A. Faessler, S. Kusuno and G.L. Strobel, Nucl. Phys. **A203** (1973) 513
16) A.L. Fetter and J.D. Walecka, Quantum theory of many particle physics (McGraw-Hill, New York, 1971)
17) A.A. Abrikosov, L.P. Gorkov and I.E. Dzyaloshinski, Methods of quantum field theory in statistical physics (Dover, New York, 1963)
18) A.E.L. Dieperink and T. de Forest Jr., Ann. Rev. Nucl. Part. Sci. **25** (1975) 1
19) L.C. Gomes, J.D. Walecka and V.F. Weisskopf, Ann. of Phys. **3** (1958) 241
20) K. Holinde, K. Erkelenz and R. Alzetta, Nucl. Phys. **A194** (1972) 161
21) W.H. Dickhoff, Nucl. Phys. **A399** (1983) 287
22) K. Nakayama, S. Krewald and J. Speth, Phys. Lett. **B148** (1984) 399
23) P. Czerski, Ph.D. thesis, University of Tübingen, Tübingen (1984)
24) W. Hengeveld, Ph.D. thesis, Free University, Amsterdam (1986)
25) P. Czerski, W.H. Dickhoff, A. Faessler and H. Müther, Nucl. Phys. **A427** (1984) 224
26) W. Hengeveld, K. Allaart and W.H. Dickhoff, Nucl. Phys. **A435** (1985) 381
27) W. Hengeveld, W.H. Dickhoff and K. Allaart, Nucl. Phys. **A451** (1986) 269
28) P. Czerski, H. Müther, P.K. Rath, A. Faessler and W.H. Dickhoff, Nucl. Phys. **A465** (1987) 189
29) S. Drozdz, V. Klemt, J. Speth and J. Wambach, Nucl. Phys. **A451** (1986) 11
30) J.E. Wise, J.S. McCarthy, R. Altemus, B.E. Norum, R.R. Whitney, J. Heisenberg, J. Dawson and O. Schwentker, Phys. Rev. **C31** (1985) 1699
31) A.H. Wapstra and G. Audi, Nucl. Phys. **A432** (1985) 1
32) G.A. Rijsdijk, work in progress
33) P.P. Domitrovich and W.H. Dickhoff, to be published
34) K. Allaart, E. Boeker, G. Bonsignori, M. Savoia and Y.K. Gambhir, Phys. Reports **169** (1988) 209
35) G. van der Steenhoven and L. Lapikas, private communication
36) C. Mahaux, P.F. Bortignon, R.A. Broglia and C.H. Dasso, Phys. Reports **120** (1985) 1
37) D. Bonatsos and H. Müther, Nucl. Phys. **A510** (1990) 55
38) G.E. Brown and M. Rho, Nucl. Phys. **A372** (1981) 397
39) J.P. Jeukenne and C. Mahaux, Nucl. Phys. **A394** (1983) 445
40) R.D. Smith and J. Wambach, Phys. Rev. **C38** (1988) 100
41) C. Mahaux and H. Ngo, Phys. Lett. **B100** (1981) 285
42) D. Van Neck, M. Waroquier and J. Ryckebusch, to be published
43) O. Benhar, A. Fabrocini and S. Fantoni, Phys. Rev. **C41** (1990) R24
44) C. Mahaux and R. Sartor, Nucl. Phys. **A503** (1989) 525
45) P. Czerski, W.H. Dickhoff, A. Faessler and H. Müther, Phys. Rev. **C33** (1986) 1753
46) E.N.M. Quint, B.M. Barnett, A.M. van den Berg, J.F.J. van den Brand, H. Clement, R. Ent, B. Frois, D. Goutte, P. Grabmayr, J.W.A. den Herder, E. Jans, G.J. Kramer, J.B.J.M. Lanen, L. Lapikas, H. Nann, G. van der Steenhoven, P. Grabmayr, G.J. Wagner and P.K.A. de Witt Huberts, Phys. Rev. Lett. **58** (1987) 1088
47) P. Whitlock and R.M. Panoff, Can. J. Phys. **65** (1987) 1409
48) L.D. Landau, Sov. Phys. **8** (1958) 70
49) W.H. Dickhoff, P.P. Domitrovich, A. Polls and A. Ramos, in Condensed matter theories, vol. 5, (Plenum, New York, 1990) p. 275
50) W.H. Dickhoff, P.P. Domitrovich, K. Allaart, M.G.E. Brand, F.A. Muller, G.A. Rijsdijk, A. Polls and A. Ramos, in Topical workshop on two nucleon reactions, Proc. EIPC vol. 3 (Giardini, Pisa, 1990), in press